UiT The Arctic University of Norway

Faculty of Health Sciences

Identification and semi-quantitative analysis of lipids in the diatom *Porosira glacialis*

Kristine Haugland

Master's thesis in Pharmacy, May 2022

Acknowledgement

The work presented in this thesis was performed at the Natural Products and Medicinal Chemistry Research Group, Department of Pharmacy (IFA), UiT The Arctic University of Norway in collaboration with the Norwegian College of Fishery Science (NFH). This work was carried out in the period from August 2021 to May 2022.

First of all, I would like to thank my main supervisor Terje Vasskog for your assistance and support throughout this period. Thank you for always finding time to help me. This thesis would not have been possible without your help.

I would like to thank my co-supervisor Torbjørn Myhre for all the help with LipidSearch and the statistics. Thank you for sharing your knowledge and for always being patient to me.

I would also like to thank my co-supervisor Lars Dalheim for letting me participate in the cultivation and harvesting process. Thank you for helping me with the biology part of the thesis. Thanks to Jon B. Svenning who helped me with the lipid extraction.

Finally, I would like to thank my classmate Agnethe, who worked with pigment analysis in microalgae. The cultivation and harvesting were performed in collaboration with her. Thank you for always being a good partner at the lab, for your good company and support.

Tromsø, May 2022

Kristine Haugland

Abstract

Background: In 2015, The University of Tromsø initiated a project with local industry involving cultivation of marine microalgae to reduce industrial CO_2-emissions. Marine microalgae are primary producers with high capacity for carbon fixation into biomass rich in lipids. Their lipid composition is characterized by high content of PUFAs such as EPA (20:5) and DHA (22:6). The biomass can potentially be utilized as supplement to marine raw materials in fish feed for aquaculture industry. To maximize the yield of lipids rich in EPA and DHA, this thesis investigates cultivation in different lighting conditions and their influence on lipid composition and fatty acid content of EPA and DHA in marine microalgae.

Method: The diatom species, *Porosira glacialis*, was exposed to red, blue and white light conditions during four days of cultivation. After harvesting, the biomass was freeze-dried and homogenized. The lipids were extracted from the biomass by a modified Folch method (DCM/MeOH) and applied to High Performance Liquid Chromatography – Mass Spectrometry (HPLC-MS) for lipid analysis in positive and negative ionization mode. AcquireX was used for data dependent acquisition to generate data of identification and relative contents of lipids and fatty acids. Identification and semi-quantitative analysis of positively charged lipids were performed by LipidSearch software, whereas manual identification was performed for SQDG, a negatively charged lipid.

Results: The major content of EPA was seen in PC, where the cultures exposed to blue and white light showed significantly increased EPA content compared to red light. For the overall content of EPA, an even distribution was observed between the different lighting conditions. The major contents of DHA were seen in PC and PE, PC having significantly higher DHA content in red and white light and PE having significantly higher DHA content in blue and red light. For the overall content of DHA, there were only significant finding between red and blue light, with the culture in red light having the highest DHA content.

Conclusion: The blue and white lighting conditions seem promising to maximize the yield of lipids rich in EPA for *P. glacialis*. However, the findings are not as clear for DHA, but a suggestion might be red light before blue light to maximize the content of DHA.

Table of Contents

Abbreviations

AA	Arachidonic acid
ACN	Acetonitrile
ALA	Alpha-linolenic acid
API	Atmospheric pressure ionization
a.u.	Arbitrary units
AUC	Area under the curve
CID	Collision induced dissociation
Chl a	Chlorophyll a
DCM	Dichloromethane
DDA	Data dependent acquisition
DGDG	Digalactosyldiacylglycerol
DHA	Docosahexaenoic acid
ESI	Electrospray ionization
EPA	Eicosapentaenoic acid
FA	Formic acid
HCD	Higher energy collisional dissociation
H-ESI	Heated-electrospray ionization
HPLC	High Performance Liquid Chromatography
HPLC-MS	High Performance Liquid Chromatography – Mass Spectrometry
HRAM	High resolution accurate mass

LA	Linolenic acid
LC-PUFA	Long-chain polyunsaturated fatty acid
MeOH	Methanol
MGDG	Monogalactosyldiacylglycerol
MS	Mass spectrometry
MUFA	Monounsaturated fatty acid
m/z	Mass-to-charge ratio
NH_4FA	Ammonium formate
PA	Phosphatidic acid
PC	Phosphatidylcholine
PE	Phosphatidylethanolamine
PG	Phosphatidylglycerol
PI	Phosphatidylinositol
PS	Phosphatidylserine
PUFA	Polyunsaturated fatty acid
Qc	Quality control
RF	Radiofrequency
RSD	Relative standard deviation
RT	Retention time
SD	Standard deviation
SQDG	Sulfolipid sulfoquinovosyldiacylglycerol

TG	Triacylglycerol
TLC	Total lipid content
UPLC	Ultra performance liquid chromatography
UiT	The University of Tromsø

1 Introduction

1.1 Background

Over the last decades, Norway has become one of the world's largest producers of farmed salmon. In 2019, Norway sold around 1.4 million tons of farmed salmon (1), which means that salmon and seafood have become the largest export product after oil and gas (2). Such a great demand has led to an ever-increasing need for salmon feed, and as a result plant ingredients like soy and rape have been incorporated in the diet. However, in recent years there have been large changes in the feed composition of the salmon diet. In 1990, the diet consisted of approximately 90% marine raw materials. Today the farmed salmon is raised on a diet consisting of around 70% plant-based materials, while only 25% of the diet remains as marine raw materials (3). Such a pronounced reduction of marine raw material in the feed composition, has led to a changed lipid profile in the salmon, with decreased amounts of the omega-3 fatty acids eicosapentaenoic acid (EPA) and docosahexaenoic acid (DHA) (4).

There is reason to believe that including high ratios of plant-based ingredients in the feed may influence the physiology of the salmon to a large extent. Plant based ingredients contain more of the monounsaturated fatty acids (MUFAs) and the short chain polyunsaturated fatty acids (PUFAs) which are rich in omega-6 fatty acids, compared to fatty acids in fish and microalgae that are rich in omega-3 fatty acids. Fish as well as mammals should include marine products in their diet to cover their need for essential omega-3 PUFAs. Research has shown that to maintain good growth performances the salmon should have an intake of at least 10 g of EPA or DHA per kilo feed (5). In a study from Torstensen et al., the growth performances of Atlantic salmon were reduced by 9%, as 80% of fish meal and 70% of fish oil were replaced by terrestrial plant proteins and oils, respectively (6). Additionally, studies on effects on gene expression in salmon tissues show changes in both intestine, liver and skeletal muscles (7-9). Among them there are physiological changes in immune and stress related processes, protein, lipid and energy metabolism, and gene expressions related to cell proliferation and apoptosis (7;8).

In addition to concerns about the welfare of farmed salmon, it becomes necessary to search for alternative sources of marine omega-3 fatty acids. Marine microalgae are a diverse group of primary producers that utilize sunlight and CO_2 to produce biomass containing PUFAs, which include the omega-3 fatty acids EPA and DHA. These organisms have shown promising potential as a supplement to marine ingredients in feed for farmed salmon. Diatoms are the

most important primary producers across Norwegian waters and can be utilized in commercial mass cultivation. One of these diatoms is *Porosira glacialis* which is a robust species capable of high production of EPA and DHA.

The University of Tromsø (UiT), initiated a project in 2015 together with local industry, where *P. glacialis* from Norwegian waters are utilized to reduce industrial CO_2-emissions. The diatom is capable to recycle CO_2 from flue gas, which may lead to large-scale cultivation of biomass rich in PUFAs, which can be used as supplement for marine raw materials in salmon feed. Optimizing the cultivation conditions for *P. glacialis*, is essential for the development of new marine raw materials to ensure a sustainable future for Norwegian salmon production. As the microalgae photosynthesis is dependent on light intensity, it is of interest to understand if different lighting conditions will influence the overall biomass production. In a previous master thesis, Myhre focused on different lighting conditions and their impact on growth rate and lipid composition (10). As this was performed in a small-scale, by cultivation in four liter flasks, a natural continuation was to investigate the lighting conditions in a scale that can reflect production in an industrial scale. In this thesis there were performed semi-quantitative analysis and identification of lipids in *P. glacialis* to investigate the lipid content of EPA and DHA.

1.2 Lipids

Lipids are a diverse group of natural occurring organic compounds, characterized by their insoluble nature in water and their solubility in organic solvents. Fatty acids, phospholipids, triacyclglycerols and steroids are some examples of different lipids. They can be classified according to their polarity, where some of them consist of structures with polar head-groups, while others are completely non-polar. The lipid compounds have vital functions in the body as building blocks in cell membranes, they function as energy storages and they also work as signal molecules.

1.2.1 Fatty acids

Fatty acids are some of the most abundant components in lipids, where they contribute to physical and metabolic properties (11). They also exist as free fatty acids, released from the storage lipid triacylglycerol (TG) as energy and structural components for the cells. The fatty acids are known for their long hydrocarbon chains with hydrophobic character and their hydrophilic carboxyl group. When solved in aqueous solutions, the carboxyl group is negatively charged and reactive. Because of the two different regions in the molecule, the fatty acids become amphipathic.

The composition of the hydrocarbon chain comprises classes of saturated- and unsaturated fatty acids. Saturated fatty acids have chains with maximal number of hydrogen atoms, and no place for any double bond. In unsaturated fatty acids, one or more double bonds are present in the chain, which is the reason why *cis*-isomers of unsaturated fatty acids have a more bended structure compared to saturated fatty acids. This also affects the melting point, which is seen to increase with a higher ratio of saturated to unsaturated fatty acids (12).

Fatty acids with only one double bond in the hydrocarbon chain are named monounsaturated fatty acids (MUFAs). Polyunsaturated fatty acids (PUFAs) have two or more double bonds in their hydrocarbon chain. Some of the PUFAs are essential like the omega-3 fatty acids eicosapentaenoic acid (EPA) and docosahexaenoic acid (DHA).

1.2.1.1 Nomenclature of fatty acids

The fatty acids are labeled after the length of their hydrocarbon chain, number of double bonds and the location of double bonds in the molecule. This gives a formula for naming the fatty acids (C:D n-p). C corresponds to the number of carbons in the molecule, while D is the number of double bonds. n-p corresponds to the number of carbons from the omega end of the molecule to the position of the first double bond. Another way to express the fatty acid nomenclature is to start from the carboxyl end (delta end) and identify the number of carbon atoms.

To give an example, DHA has a chain length of 22 carbon atoms and six double bonds. The double bonds start between the third and fourth carbon from the omega end and continues to the last double bond between the eighteenth and nineteenth carbon. With this nomenclature DHA will be named 22:6 n-3, where this assumes that each double bond is separated by a CH_2-group.

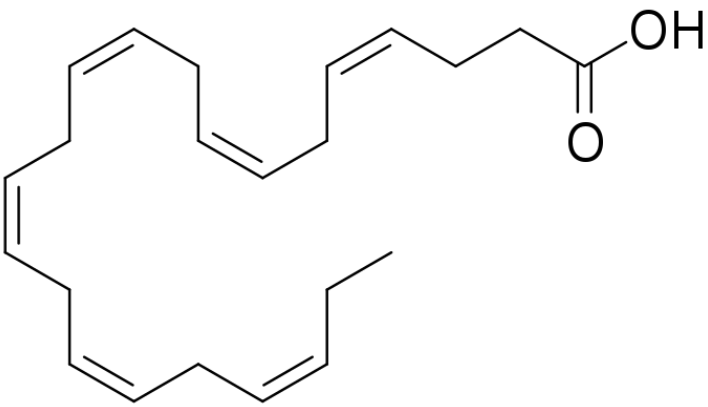

Figure 1 – Docosahexaenoic acid (DHA) (22:6 n-3).
https://commons.wikimedia.org/wiki/File:Docosahexaenoic_acid_structure.svg

1.2.2 Acylglycerols

Acylglycerols are lipids made up of a glycerol molecule and fatty acids. The hydroxyl groups on glycerol are linked to the fatty acids through an ester bond. Acylglycerols can be either mono-, di- or triacylglycerols dependent on how many fatty acids are connected. These non-polar compounds are present as lipoproteins in the blood plasma and stored in fat deposits. Triacylglycerol (TG) function as the primary energy storage of long-chain fatty acids in the cell, and when energy is required, fatty acids are released initiated by a hydrolysis reaction.

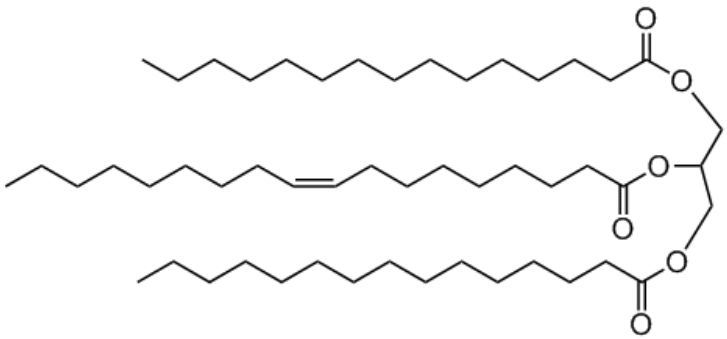

Figure 2 –Triacylglycerol (TAG) 15:0/18:1/15:0. Photo credit: avantilipids.com

1.2.3 Phospholipids

The structure of phospholipids closely relates to TG. The glycerol molecule is linked to two fatty acids and a phosphoric acid. The phosphate group is ionized with a negative charge and is often linked to other hydrophilic molecules such as choline. This result in an amphipathic molecule with a hydrophilic head group and hydrophobic tail, which has an important function in construction of the cell membrane. Some examples of phospholipids are phosphatidylcholine (PC), phosphatidic acid (PA) and phosphatidylserine (PS).

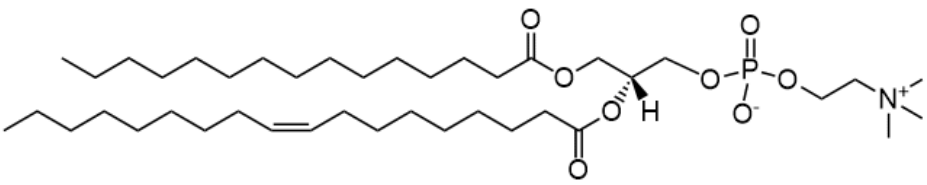

Figure 3 - Phosphatidylcholine (PC) (15:0/18:1 n-9). Photo credit: avantilipids.com

1.2.4 Glycolipids

Glycolipids consists of one or two fatty acids conjugated to a carbohydrate by a glycosidic bond. The polar carbohydrate group can either be monosaccharide or oligosaccharide and is linked to a glycerol backbone. With their amphipathic nature, they become an important part of the phospholipid bilayer stabilizing the cell membrane and contribute to cell-to-cell interactions. Monogalactosyldiacylglycerol (MGDG) and digalactosyldiacylglycerol (DGDG) are the most abundant glycolipids in microalgae. They can be found in thylakoid membranes in chloroplasts where photosynthetic activity takes place (11). MGDG and DGDG are known for their high content of PUFAs, including the omega-3 fatty acid, eicosapentaenoic acid (EPA) (13).

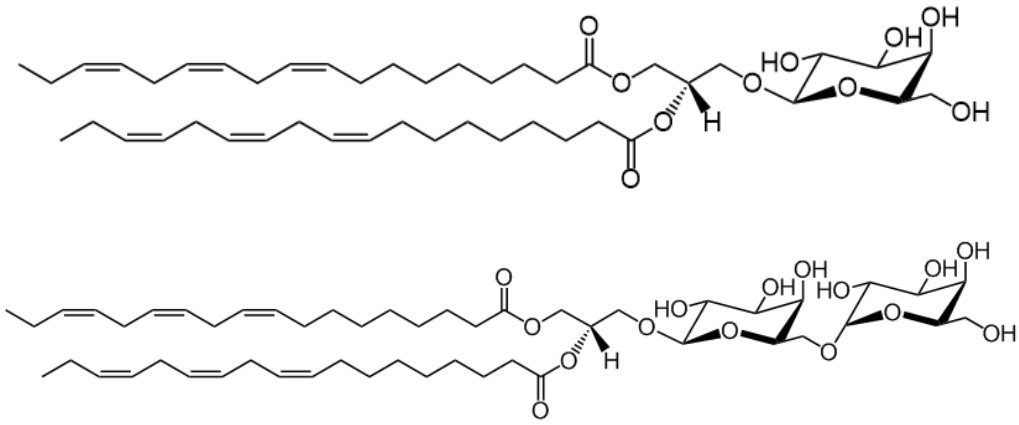

Figure 4 - Monogalactosyldiacylglycerol (MGDG) 18:3/18:3 (top). Digalactosyldiacylglycerol (DGDG) 18:3/18:3, (bottom). Photo credit: avantilipids.com

1.2.5 Sulfolipids

Together with DGDG and MGDG, sulfolipids such as sulfoquinovosyl diacylglycerol (SQDG) is a primary constituent of the thylakoid membrane in plants, microalgae and bacteria. SQDG consist of a polar sulfoquinovose headgroup connected to the glycerol backbone together with two non-polar fatty acyl chains. With its anionic nature, SQDG contribute to stabilize the negative charges of the membrane. The biological function of SQDG is only partly understood, but it can seem to be involved in cell signaling and sulfur storage in cells. High contents of PUFAs such as EPA and DHA are seen in this lipid class (13-15).

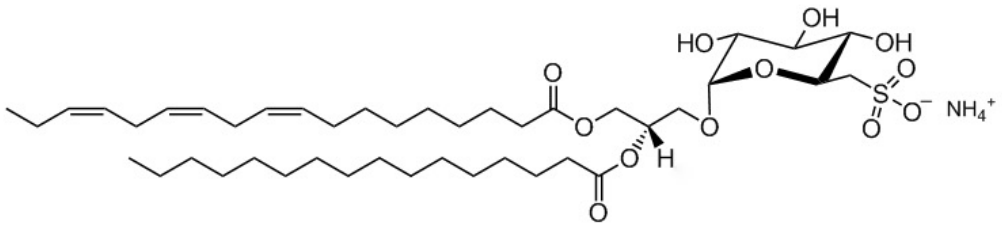

Figure 5 - Sulfoquinovosyl diacylglycerol (SQDG) 16:0/18:3. Photo credit: avantilipids.com

1.2.6 PUFAs

Both mammals and fish have limited capacity to synthesize omega-3 and omega-6 PUFAs from fatty acids in the body. These PUFAs are essential constituents of the cell membrane and function as precursors for several substances in the body. As well they have important functions in growth and repair. The omega-3 fatty acids are recognized by their first double bond between the third and fourth carbon atom from the omega end of the fatty acid chain, while the omega-6 fatty acids have the first double bond placed between the sixth and seventh carbon atom. There are several different omega-3 fatty acids, but the most common are alpha-linolenic acid (ALA, 18:3 n-3), eicosapentaenoic acid (EPA, 20:5 n-3) and docosahexaenoic acid (DHA, 22:6 n-3). The precursor for the omega-6 fatty acids is linolenic acid (LA, 18:2 n-3), which among other things can be converted into arachidonic acid (AA, 20:4 n-6). Both EPA and DHA can be synthesized from ALA, but this process is limited. EPA and DHA are therefore recommended to be included directly in the diet. Phytoplankton and marine algae are today considered as the principle sources of omega-3 fatty acids (16).

Today it is widely known that the PUFAs serve beneficial effects for public health. The omega-3 fatty acids are important in maintaining normal metabolic function, for cognitive function, and for growth and development. They show anti-inflammatory activity by regulation of the eicosanoids in the body. Dietary intake of omega-3 fatty acids contribute to decrease the plasma TG levels, lower the blood pressure and reduce the risks of coronary heart disease (17 p. 362-364). In contrast to the omega-3, the omega-6 fatty acids show both anti-inflammatory and pro-inflammatory effects. When substituted for saturated fats, omega-6 fatty acids both decrease plasma LDL and HDL cholesterol (17 p. 362-364). Although, high levels of omega-6 fatty acids have shown incidences of increased risks of obesity, type II diabetes and heart disease (16).

The production of omega-3 and omega-6 fatty acids follow two distinct metabolic pathways, with ALA as precursor for EPA and DHA, and LA as precursor for AA. There are no connections that allow omega-6 to be converted into omega-3 fatty acids. The only connection is that these essential fatty acids compete for the same metabolic enzymes. This means that an increased dietary intake of EPA and DHA will partially replace the omega-6 fatty acids in the cell membrane, and vice versa. According to the health benefits of PUFAs, a high omega-6/omega-3 ratio will lead to an increased production of eicosanoids from AA, which is inconvenient as these eicosanoids have shown to be biologically active in very small quantities, which will increase the risks of for example thrombosis (18).

1.3 Diatoms

Diatoms are photosynthetic eukaryotic organisms found in freshwater as well as seawater, and account for around 40% of total aquatic primary production (19). They make up the largest group of microalgae and are the dominant primary producers in the spring bloom in Norwegian waters (20 p. 11). Diatoms have a cell size varying from two micrometers to two millimeters. They are characterized by their frustule, a cell wall made up of silica, which encase the whole microalgae. The frustule can be present in various symmetrical shapes, where the centric diatoms have circular shapes (Figure 6) and the more common pennate diatoms have elongate and bilaterally symmetric shapes (Figure 7) (21 p. 271). Diatoms are mainly organized as single cells, but they also occur in chains or colonies (22).

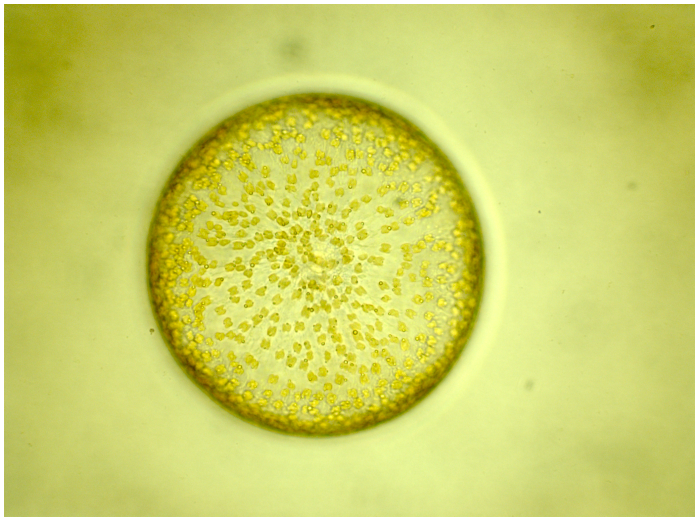

Figure 6 - *Coscinodiscus* sp. Example of a centric diatom. Photo credit: Svenning, Jon B.

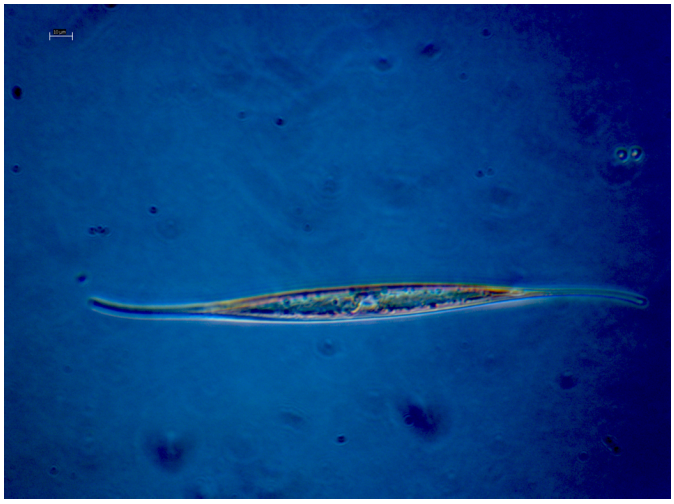

Figure 7 - *Gyrosigma tenuirostrum*. Example of a pennate diatom. Photo credit: Eriksen, Gunilla K.

For photosynthetic activity, the diatoms need dissolved CO_2 and sunlight which is absorbed by the pigments. In the oceans, photosynthetic activity appears in the euphotic zone, where net photosynthesis exceeds respiration (23). Diatoms also require macronutrients such as nitrogen and phosphorus, as well as trace metals. Silicic acid is required as a building block for the frustule (24). Under optimum growth conditions, diatoms will continue with binary fission at a constant rate, this is known as the exponential growth phase (25). Under unfavorable growth conditions, particularly deficiency of nitrogen, the growth rate gradually slows down into a stationary phase and energy storage as lipids (26).

The lipid composition of diatoms has been extensively studied due to their high capacity for carbon fixation through photoautotrophic growth and storage of carbon in the form of lipids, which make the microalgae a potential source for the production of biodiesel (19;27). The fatty acid composition in diatoms is dominated by 14:0, 16:0, 16:1n-7 and PUFAs such as 16:2n-4, 16:3n-3, 16:4n-1 and EPA, whereas DHA is present in minor amounts. The photosynthetic thylakoid membrane mainly consists of the glycolipids MGDG and DGDG, with minor amounts of SQDG. Diatoms also contain phospholipids such as phosphatidylcholine (PC), phosphatidylethanolamine (PE), phosphatidylglycerol (PG), as well as phosphatidylserine (PS) and phosphatidylinositol (PI) (27). During limited nutrient conditions, these microalgae have the ability to alter their biosynthesis of lipids into production and accumulation of TG in their stationary growth phase (26).

1.3.1 Porosira glacialis

Through this project, the diatom species *Porosira glacialis* has been studied (Figure 8). The Arctic species belongs to the family Thalassiosiraceae. *P. glacialis* has a diameter of about 30-40 micrometers, where the cells may be connected in chains. They can be found early in the arctic spring bloom and are spread across the Norwegian coastal waters (20 p. 130). The lipid composition of *P. glacialis* has been investigated by Svenning et al., showing a preference for MGDG, DGDG, PG and PC, and high content of PUFA in the form of EPA when harvested in the exponential growth phase (27). With such a lipid composition, *P. glacialis* may be a valuable source as supplemental ingredients for the fish feed industry.

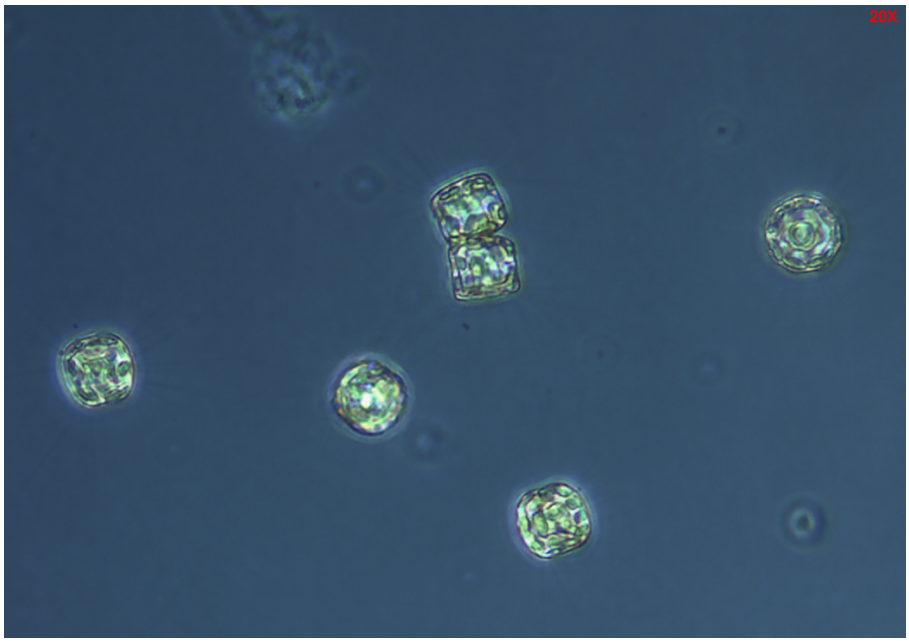

Figure 8 - *Porosira glacialis*. Photo credit: Bæverud, Agnethe H.

1.4 Lipid extraction

Sample preparation of diatom biomass for lipid analysis involve the use of extraction methods to release lipids present in the microalgal cell membrane and in adiposomes inside the cell (28). There are several options of extraction methods, but they deviate in lipid yield. In 1957, Folch et al developed an extraction method which has become the preferred method when dealing with lipid extraction and microalgae, due to its large lipid yield (29).

In order to extract the lipids, the biomass needs to be homogenized. It is common to use freeze dried material from the microalgae to avoid microbial growth and chemical degradation. Freeze dried material is also an advantage when comparing lipid content in different biomass-samples, as it eliminates challenges with different content of water in different microalgal biomasses. Homogenized biomass is extracted with a solvent mixture of chloroform and methanol (2:1), to a final dilution 20-fold the volume of the biomass sample, where one gram of biomass is added 20 ml of chloroform-methanol (2:1). The recent years it has been common to modify the method with dichloromethane as extractant instead of chloroform, to reduce the health risks. In the purification step, water or a solution of mineral salts, is added to the filtrate of biomass and solvents to achieve a biphasic system. The lower phase contains lipids and non-polar substances, while the upper phase is aqueous. In the Folch extraction method, only a negligible fraction of lipids is lost to the aqueous phase (30).

There have been discussions if cell disruption influences the lipid yield. A study of the diatom *P. glacialis* by Svenning et al., showed no considerable lipid yield increase when cell disruption was performed as a separate process prior to the extraction (31). Another subject that should be discussed is accomplishment of the extraction in large-scale production such as the fishing industry, and the consideration of utilizing solvents in a health- and cost perspective. In a previous master thesis, Stabell investigated lipid yield from herring roe for lipid extraction by "green technology", where ethanol and heptane/isopropanol were substituted for dichloromethane/methanol which is normally used in the Folch extraction method. The project showed promising results for a healthier production, with increased lipid yield for lipid extraction with ethanol as extractant, but no statistical analysis were applied in the study (32).

1.5 Lipidomics

The definition of lipidomics emerged in 2003 as the study of processes and networks of the complete cellular lipid profile in biological systems (33). Lipidomic analysis is performed by advanced instrumentation such as high resolution and/or tandem mass spectrometry (MS), which have been important for the development of lipidomics. MS can be used in combination with chromatographic separation techniques (LC-MS) to better understand the diversity of physico-chemical properties of lipid compounds. By implementing such analytical methods, it is possible to identify and quantify lipid species from various lipid classes, subclasses and categories. Lipidomics has become an important analytical tool for identifications of biomarkers of disease and disease mechanisms, as well as diagnostics for several serious diseases within cardiovascular diseases, cancer diseases or neurological disorders (34;35).

1.6 Analytical techniques

Today High Performance Liquid Chromatography – Mass Spectrometry (HPLC-MS) is the leading analytical technique in lipidomics, with properties as high resolution, high mass accuracy and fast run times. The technique allows combination of chromatography, where compounds are separated from each other according to their physicochemical properties, with mass spectrometry, where separated compounds are identified based on their mass-to-charge ratio (*m/z*).

1.6.1 High performance liquid chromatography

High performance liquid chromatography (HPLC) is a chromatographic technique where components in a mixture are separated based on interactions between particles in a column and analytes in a solution. The sample, consisting of analytes and matrix, is injected and dissolved into a liquid mobile phase, which carries the sample through a solid stationary phase column with a constant flow (Figure 9). Different sample components have different affinity for the stationary phase particles, and because of the equilibrium distribution the components will distribute differently between the mobile phase and the stationary phase. Physical and chemical characteristics of the mobile phase and stationary phase, in addition to temperature, are some parameters affecting the interaction and the distribution. As a result, the components will

separate from each other as they elute at different times from the column. This is registered by a detector in the end of the column as retention time (RT). The detector response is presented in a chromatogram as signals based on RT and relative intensity.

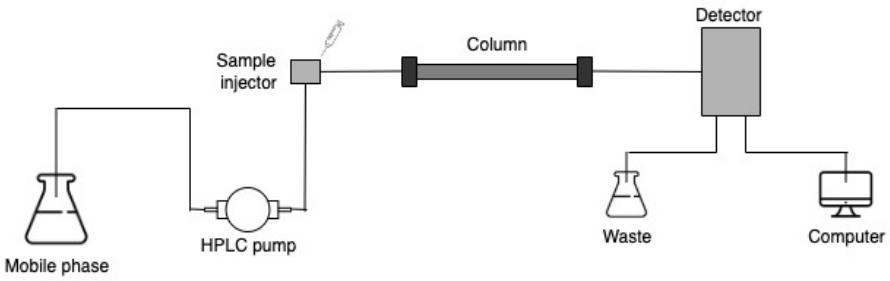

Figure 9 - Schematic representation of a HPLC setup. Figure created in diagrams.net

Standard HPLC columns have an inner diameter of 2-5 mm and a length of 3-25 cm. The particle size of the stationary phase is typically around 3-5 µm. Today ultra performance liquid chromatography (UPLC) has become popular for lipidomic analysis due to faster analysis, high resolution, lower detection limits and less expended mobile phase. The columns used for UPLC are often shorter, with a length of 3-10 cm, and a stationary phase particle size less than 3 µm. They show the same efficiency as the HPLC columns and are ideal when running large amounts of samples. Robustness is a prerequisite for UPLC columns, and pumps, as smaller particle size cause high back pressure.

1.6.1.1 Stationary phase

Conventional HPLC columns are packed with spherical and porous silica particles. Uniformity of the particles is desirable as it contributes to less band with. Modifications are performed to the silica particles to achieve desired interactions between analytes and the stationary phase. Due to significant non-polar nature and relatively large size of lipid molecules, reversed phase columns with hydrophobic stationary phase are most used in lipidomic analysis. Reversed phase chromatography uses silica particles modified by hydrophobic reagents such as octadecyl, a hydrocarbon chain with 18 carbon atoms (C18), linked to the silanol groups. In addition, it is common to treat the silanol groups with trimethylchlorosilane to prevent unwanted interactions due to steric hindrance (36 p. 148-149). For reversed phase columns, the

chromatography is based on hydrophobic interactions with van der Waals forces as the main interaction forces.

1.6.1.2 Mobile phase

In reversed phase chromatography, the mobile phase is a mixture of water and organic solvent, with a hydrophilic character. By adding more organic solvent the strength of the mobile phase increases and vice versa. By increasing the amount of strong mobile phase, the interaction between the analyte and the stationary phase will be reduced, the solubility of the analyte in the mobile phase will increase, leading to shorter retention times. Acetonitrile (ACN) and isopropanol are among the strongest organic solvents used in reverse phase. In lipidomics it is common to use strong mobile phases, due to strong hydrophobic interactions between lipids and the stationary phase.

The mobile phase composition can either be constant through the analysis, isocratic elution, or graded for a defined time window, gradient elution. Gradient elution makes it possible to adjust the analysis in proportion to the retention time profile of the analytes, thus reduce time of analysis and ensure narrow peaks. In addition, the mobile phase composition can be adjusted by adding small amounts of buffer solutions to regulate the pH, for better chromatographic quality and ion pair formation (37).

1.6.2 Mass spectrometry

Mass spectrometry (MS) is an analytical technique utilised for *m/z* measurements of chemical compounds. This can provide information about molecular weight, elemental composition and functional groups. The information can be used for identification of unknown compounds, as well as for quantitative analysis (36 p. 233).

The mass spectrometer consists of an ion source, a mass analyzer, an ion detection system and some also have a collision cell. If used as a detector for UPLC, the UPLC column function as an inlet to introduce separated compounds to the ion source. In the ion source the compounds are ionized, which result in formation of molecular ions and fragment ions, if the molecular ions decompose. Formation of adduct ions may also occur. The ions are transported to the mass analyzer where the ions are measured according to their *m/z* -values. The occurrence of

measured ions is registered by an ion detection system and the results are presented graphically in a mass spectrum, with *m/z* against relative intensity.

1.6.2.1 Ion source

A requirement for using MS as an analytical method is that the molecules have at least one charge. Positively and negatively charged molecules can be manipulated by external electrical and magnetic fields (38). While neutral molecules move in straight lines, ions subjected to an external field will follow specific trajectories. Electrospray ionization (ESI) is a widely used ionization technique in HPLC-MS (36 p. 246). ESI is a soft ionization technique performed under atmospheric pressure outside the low-pressure chamber of the instrument. The ionization source produces mainly intact molecular ions, and with optimized source conditions only a little in-source fragmentation may occur.

The sample, which is in a solution with the mobile phase in the UPLC column, is delivered with a low flow rate to a narrow metal capillary in the ionization source. A drying gas, for instance nitrogen, assists atomizing the solution into an aerosol of small droplets. An electrical potential from a power supply adds positive or negative voltage to the end of the capillary, and as a result the droplets become charged. The analytes can be protonated or deprotonated, or if other ions are present in the mobile phase, adducts such as Na^+, NH_4^+ or COO^- can be created. As the mobile phase evaporate and the electrical potential increase according to the droplet size, the analyte molecules are released from the droplets as ions and transferred to the MS.

1.6.2.2 Mass filter

The quadrupole is a widely used mass filter in MS. It is made up of four parallel cylindrical metal rods which are exposed to an alternating electrical field. Opposing rods are electrically connected in pairs around a central axis. Ions follow different trajectory paths according to their *m/z* ratio, and by changing the radiofrequency (RF) of the electrical field, ions with a certain *m/z* value will pass through the quadrupole, while ions with unstable trajectories are filtered out. As a mass filter, the quadrupole can be used to select precursor ions for further fragmentation.

1.6.2.3 Ion detection system

Since the commercial introduction of the Orbitrap mass analyzer in 2005, the instrument has become famous for its high mass measurement accuracy (2-5 ppm), high mass resolution (100 000 – 1 000 000 FWHM) and high dynamic range. The orbitrap is composed of an axial central electrode and a coaxial outer electrode. An electrostatic field, capable of capturing incoming ion packets, is created between the symmetrical electrodes. Stable ion trajectories direct ions in rotations around the central electrode and axial oscillations along it in the form of rings. The frequency of circular trajectories and axial oscillations are detected and converted into *m/z* values by Fourier transform (39;40).

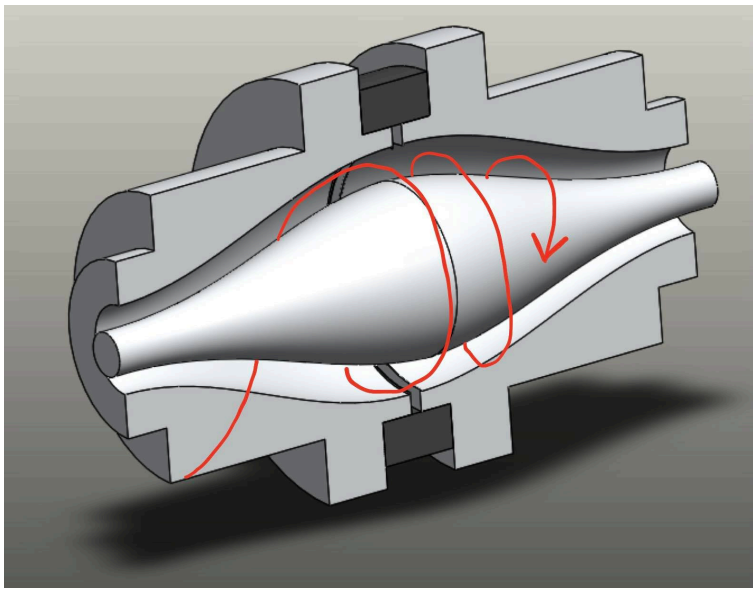

Figure 10 – Ion oscillations in Orbitrap mass analyzer. Figure credit: Haugland, Anders

1.6.2.4 Ion trap

The linear ion trap is a device that can function as a mass filter, a collision cell for fragmentation and a mass analyzer for both precursor- and fragment ions. The ion trap consists of a set of quadrupole rods surrounded by a ring electrode and confined by two endcap electrodes. By varying the voltage applied to the electrodes, it has the ability to store and focus ions into stable trajectories based on their *m/z* values. Inside the ion trap a buffer gas attend to focus the ions into stable trajectories as well as it serves as a collision gas for fragmentation.

1.6.2.5 *Orbitrap ID-X Tribrid Mass Spectrometer*

For identification of complex samples high resolution accurate mass (HRAM) MS instruments are required. For this purpose, Thermo Fisher Scientific developed the *Orbitrap ID-X Tribrid mass spectrometer*, a combination of a quadrupole mass filter, a collision cell, the orbitrap mass analyzer and a linear ion trap (Figure 11). Fragmentation is performed either in the collision cell inside the linear ion trap or in the HCD cell in the ion routing multipole. The instrument has a width of mass resolution levels from 7500 to 500 000 FWHM.

The tribrid instrument is connected to an ion transfer system (S-lens) for transmission of ions from the atmospheric pressure ionization (API) source, configured in heated-electrospray ionization (H-ESI) mode, to the quadrupole. By an active beam guide, neutral components are prevented from entering the quadrupole as their motions do not follow the curved shape of the device. Both the quadrupole mass filter and the linear ion trap can be set to perform precursor ion selections within a mass range of *m/z* 50 to 2000 (normal *m/z* range mode). Selected precursor ions are collected and stored as ion packages in the C-trap. When the ion package has reached a pre-defined amount- or time limit, it is either injected for fragmentation into an ion-routing multipole (MS^2), into a linear ion trap for in depth fragmentation (MS^3) or directly into the orbitrap for mass scans. Ion packages is a requirement for full scan analysis in the orbitrap, as the instrument is not compatible for continuous scans. In need for several fragmentations (MS^2/MS^3) and faster analysis, the ions are transferred to the linear ion trap (41;42).

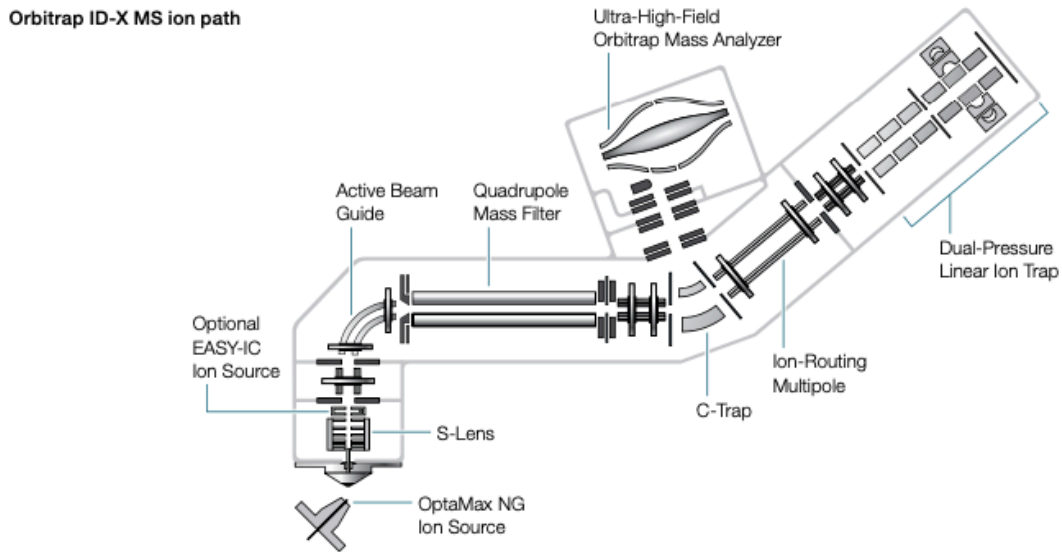

Figure 11 - Orbitrap ID-X Tribrid Mass Spectrometer. Photo credit: Thermo Fisher Scientific (41).

1.6.3 MS^n fragmentation

Fragmentation is a valuable molecular dissociation technique used to gain information about structural composition of complex compounds. If precursor ions are unstable, chemical bonds can be broken and the molecule cleaved into smaller fragments, which makes it possible to analyze several peaks in the mass spectrum that corresponds to a precursor ion. In MS, fragmentation takes place in collision cells as precursor ions collide with an inert collision gas. The fragmentation patterns can be compared with a theoretical fragmentation pattern or a database, and are essential for identification. Since lipids are composed of specific building blocks, they will follow specific and predictable fragmentation pathways, which makes analysis of MS^n fragmentation data of lipids relatively simple (43).

For the *Orbitrap I*D-*X Tribrid Mass Spectrometer,* fragmentation takes place in two different collision cells. In the ion routing multipole, fragmentation is induced by applied RF voltage and collisions with remaining nitrogen molecules from bath gas introduced from the C-trap (44). This higher energy collisional dissociation (HCD) fragments all ions introduced to the collision cell, where fragmentations may occur several times to the precursor ions and the fragment ions. The linear ion trap also functions as a collision cell. By collision induced dissociation (CID), MS^2 and MS^3 fragmentations are possible by selective selection of precursor ions and/or product ions. This is a softer fragmentation technique based on vibrational pathways, where gas collisions with helium contribute to increase internal energy of ions (42;45).

1.7 Identification of lipids

1.7.1 AcquireX

AcquireX from Thermo Fisher Scientific is a data acquisition workflow suitable to generate data of low-abundance analytes in complex samples, such as in lipidomic analysis. Through data-dependent acquisition, the workflow automatically creates exclusion lists by identifying background interference in a blank sample, made up of solvents and system impurities. Contaminants may come from the solvents themselves, the mobile phase or the LC-system. In the manner of AcquireX, full scans are performed for all individual samples, while MS^n analysis is chosen for the ID-sample, which is a pooled sample of all individual samples prepared. In order to reduce the overall run time, each precursor ion that has been fragmented is added to an exclusion list before the next analysis of the ID-sample. Several injections of the ID-sample are required to obtain full identification of complex lipid samples. Data-dependent acquisition ensures in-depth fragmentation of relevant compounds, thus increasing profile efficiency.

1.7.2 LipidSearch

The LipidSearch software is a database from Thermo Fisher Scientific used for identification and semi-quantitative analysis of lipids. It contains predicted fragmentation patterns for more than 1.5 million lipid ions. The software automatically analyses imported raw-files, which results in drastically reduced data analysis time and reduced risk of manual errors (46).

LipidSearch is programmed to search for fragmentation spectra for all precursor ions present in the ID-sample. Additionally, for each detected precursor ion the software predicts fragmentation patterns generated from a theoretical database. Product ions from the ID-samples are compared to predicted fragmentation patterns from the LipidSearch database to verify individual lipids and lipid classes. For full identification of lipids, verified MS spectra are aligned to MS spectra of the individual samples, according to accurate mass and retention time (47).

Semi-quantitative analysis is performed for precursor ions and presented as integrated peak areas in ion chromatograms for parallel measurements. By integration of the respective area under the curve (AUC), it is possible to decide the relative occurrence of identified lipids in each sample. Statistical analyzes are performed by comparative analysis between individual samples and ID-samples using t-tests, which is graphically presented as whisker-plots (48).

1.7.3 Class specific identification of SQDG

To confirm the identity of SQDG, MS^2 measurements and exact masses are required for the fragmentation patterns of the sulfoquinovosyl head group and the fatty acyl chains. Fragments originating from the sulfoquinovosyl head group are specific for the SQDG lipid class. Reports from literature describe a peak signal at *m/z* 225.0, which corresponds to the dehydrated form of the sulfoquinovosyl anion ($[C_6H_9O_7S]^-$), as a class-diagnostic product ion. The product ion originates from cleavage of an ether bond, which can be seen in Figure 12 (13;14;49-54).

Total identification of a molecular species of SQDG involve fragmentation patterns from one or two fatty acyl chains. Identification of one fatty acyl chain is sufficient to decide the total fatty acid combination, thus the last fatty acid can be decided by subtracting the identified fatty acyl chain from the total fatty acid composition. Fatty acyl chains of SQDG are mainly identified by neutral losses of fatty acids ($[M\text{-}H\text{-}RCO_2H]^-$) and the corresponding carboxylate anions ($[RCOO]^-$), but neutral losses of aldehyde ($[M\text{-}H\text{-}RCHCO]^-$) are also observed. In Figure 12, the fragmentation pathways of neutral losses of fatty acids are shown. Although there is a lot of knowledge about the fragmentation pathways for SQDG, a complete identification requires determination of the regiospecific sn-1/sn-2 positions of the fatty acyl chains, this has not been attempted through this project (13;14;54).

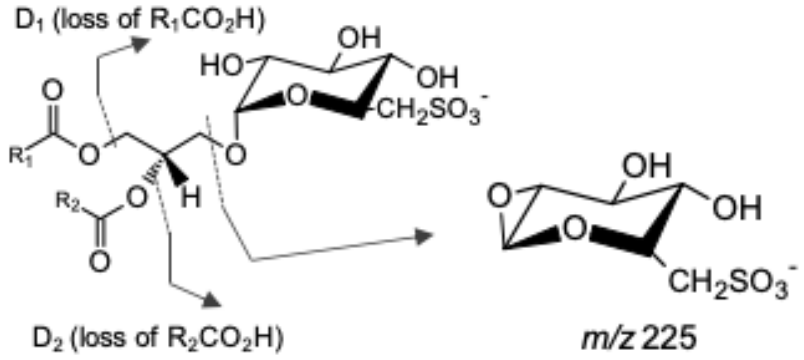

Figure 12 – Fragmentation pathways of class-specific product ion at *m/z* 225.0 and neutral losses of fatty acids ($[M\text{-}H\text{-}RCO_2H]^-$) in SQDG (13).

2 Aim of the thesis

The aim of this thesis was to investigate the lipid composition of the diatom *P. glacialis* after large-scale cultivation in three different light conditions. In addition, it was an aim to investigate which cultivation conditions that was connected to optimal yield of lipids rich in EPA and DHA.

To obtain the main aim of the thesis, several sub-goals were set:

- Investigate sample concentration according to chromatographic quality.
- Test whether analysis in negative ion mode can contribute to identification of lipid classes that can not be found in positive mode.
- Test whether LipidSearch manage to identify negatively charged lipids.
- Perform statistical analysis to investigate optimal light conditions for cultivation.
- Evaluate results from earlier small scale cultivation with the previous large scale cultivation performed outdoors.

3 Materials and methods

3.1 Chemicals

Table 1 – Chemicals and solvents for lipid extraction and LC-MS analyzes. *NaCl 5% solution was prepared at the Norwegian College of Fishery Science (NFH).

Substance	Purity	CAS-number	Supplier
Dichloromethane	≥ 99.8 %	75-09-2	Merck KGaA, Dramstadt, Germany
Methanol	≥ 99.9 %	67-56-1	VWR International, Leuven, Belgium
*NaCl 5% solution			
Milli-Q water			Millipore Corporation, Molsheim, France
2-Propanol	≥ 99.9 %	67-63-0	VWR International, Leuven, Belgium
Acetonitrile	≥ 99.9 %	75-05-8	Sigma Aldrich, St. Louis, MO, USA
Ammonium formate (NH_4FA)	≥ 99.9 %	540-69-2	Merck KGaA, Dramstadt, Germany
Formic acid (FA)	97.5 – 98.5 %	64-18-6	Merck KGaA, Dramstadt, Germany

3.1.1 Preparation of NaCl 5% solution

A sample of 50 g NaCl was weighed into a cylinder and added 1 L of Milli-Q water. The preparation took place at NFH.

3.2 Materials

Table 2 – Materials used for lipid extraction

Description	Name of equipment	Supplier
Freeze dryer	Labconco FreeZone Freeze Dry System	Labconco Corporation, Kansas City, MO, USA
Glass tubes	Kimax test tubes with Teflon Liner Caps, 13 x 100 mm, 8 mL	DWK Life Sciences, Mainz, Germany
Brown glass vials	Amber vials, screw top, 8 mL	Supelco, Bellfonte, PA, USA
LC-MS vials	Amber Screw-Top Kitpack, 12 x 32 mm, 2 mL, glass screw top vial, pre-slit, silicone/PTFE septa	Waters, Milford, MA, USA
Finntip pipettes, different sizes		Thermo Fisher Scientific, Waltham, MA, USA
Glass pipettes	Disposable Glass Pasteur Pipettes, 230 mm	VWR International, West Chester, PA, USA
Analytical balance	VWRI611-3446, ioniser for analytical and precision balance	VWR International, Leuven, Belgium
Centrifuge	Jouan C312 Benchtop Centrifuge	Thermo Fisher Scientific, Waltham, MA, USA
Nitrogen evaporator	Stuart sample concentrator SBHCONC/1	Cole-Parmer, Staffordshire, UK
Vortexer	Reax top, 5 mm, 200-3.3 rpm	Heidolph Instruments, Schwabach, Germany

3.3 Cultivation of *Porosira glacialis*

The starting point for cultivation was a monoculture of *Porosira glacialis* that was isolated from a sediment sample in the Barents Sea (N 76° 27.54′, E 033° 03.54′) in 2014. Before the cultivation, the microalgae had to acclimate for seven days with red, blue and white light (Eurolite LED IP FL-10 COB RGB). The recorded peak wavelengths for red and blue lights were 627 nm and 454 nm, respectively, and 453 nm, 627 nm and 520 nm for the white light (Figure 13). These were recorded using a BLACK-Comet Fluorescence Spectrophotometer (StellarNet, Tampa, FL, USA). After acclimatization they were diluted to different starting concentrations, where the average starting concentrations for respectively red, white and blue light were 2.7 x 10^5, 5.8 x 10^5 and 5.4 x 10^5 cells/L.

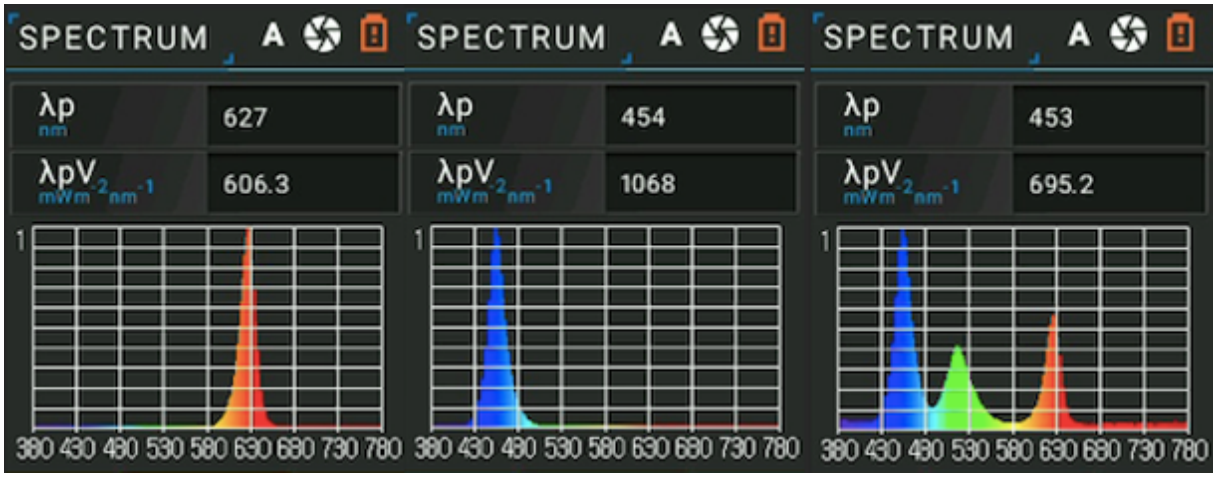

Figure 13 - Recorded peak wavelengths for red, blue and white light.

The cultivation was performed in 150 L plexiglass cylinders and distributed over nine cylinders with parallel triplicates of red, blue and white light (Figure 14). Each cultivation cylinder contained a volume of 50 L culture medium, consisting of filtered seawater, and 30 mg/L Kristalon (Kristalon Purple, Norgro) and 8.75 mg/L silicate (Sodium metasilicate 5H20, Permakem) as inorganic nutrients. A system that continuously pumps air into the bottom of the cylinders was also installed, to ensure mixing and prevent sedimentation of the microalgae. It all happened outdoors in a container, with temperatures varying from -1.8 to 5.7 °C and pH from 7.88 to 8.16. The cultivation conditions were optimized to mimic the environments for production in an industrial scale.

Figure 14 – Mass cultivation of *P. glacialis* in cylinders exposed to red, blue and white light.

3.4 Harvesting of *P. glacialis*

After four days of cultivation, the microalgae were harvested in the active growth phase by using a plankton net (KC Denmark AS, Silkeborg, Denmark) (Figure 15). Due to significantly different amounts of total biomass yield from the different lighting conditions, the culture from the red light was filtrated by a 10 μm pore sized net, while the cultures from the blue and white light were filtrated by a plankton net with pore size of 20 μm. Centrifugation tubes of 50 mL (Corning Science, Reynosa, Mexico) were washed with 96% ethanol before the filtered samples were added. The samples were centrifuged at 2576 G for five minutes (VWR Mega Star 600R, Germany). After centrifugation, the supernatants were removed before the remaining biomasses were frozen and stored at -80 °C.

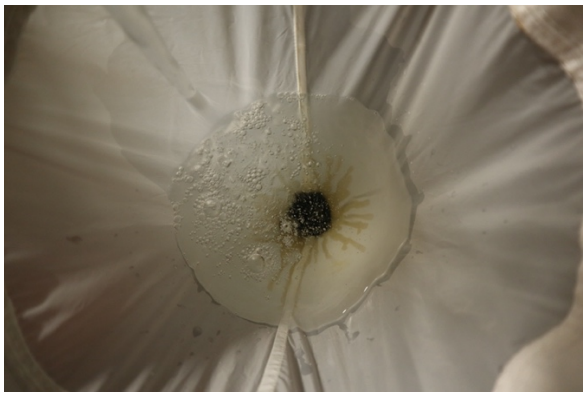

Figure 15 - Harvesting of *P. glacialis* cultivated in red light.

3.5 Lipid extraction

A modified Folch extraction method was performed at room temperature (~25 °C), with the extractants dichloromethane (DCM) and methanol (MeOH). Prior to the extraction, the microalgal biomass was freeze-dried for 24 hours and homogenized with a spatula by hand. Due to low output of biomass for the culture exposed to red light, the three parallels from red light were merged into one sample representing cultivation in red light. Biomass samples from blue and white light were kept as triplicates for each lighting condition (Table 3).

Table 3 - Overview of the modified Folch extraction method.

Lighting condition	**Microalgae material**	**Extraction**	**Parallells**
Red	50 mg	2 mL DCM:MeOH 2 mL 5% NaCl-solution	6
Blue	100 mg		18
	50 mg		
	100 mg		
White	100 mg		18
	100 mg		
	50 mg		
			Total: 42

The extraction was carried out for a total of seven samples. Sample quantity was decided in consideration of total biomass content. Glass tubes with microalgae material were combined with 2 mL DCM:MeOH (2:1 v/v) and 2 mL 5% NaCl in MilliQ water (w/v), and gently shaken by hand. To achieve optimal phase separation, the glass tubes were set to centrifugation at 2000 G for five minutes. The upper aqueous phase was discarded, while the organic phase on the bottom of the extract was transferred to a pre-weighed brown glass vial. To increase the lipid yield, the extraction was repeated. A nitrogen evaporator at 50 °C was used to evaporate the samples to dryness for 20 min, before gravimetric determination of total lipid content. Finally, the lipid content was reconstituted in isopropanol to a concentration of 1 mg/mL. Each of the seven samples were distributed with six parallels to LC-MS vials (three for analysis in positive ion mode/ three for analysis in negative ion mode) and stored at -20 °C.

3.6 Sample preparation

The sample concentration was experimentally decided in consideration of chromatography quality, where a concentration of 1 mg/mL showed to be ideal for lipid analysis. Resuspended samples with the concentration of 1 mg/ml were vortexed for ten seconds and transferred to 42 LC-MS vials, 21 samples for identification in positive ion mode and 21 samples for negative ion mode. A pooled-sample, was created by combining 170 *m*L of each resuspended sample into a LC-MS vial. It was vortexed for ten seconds. The pooled sample is used both as ID-sample and quality control sample (Qc).

In order to investigate background interference, a blank sample was created by adding 2 mL DCM:MeOH (2:1 v/v) and 2 mL 5% NaCl in MiliQ water (w/v) to a brown glass vial. After phase separation, the aqueous phase was discarded and the organic phase was evaporated in a nitrogen evaporator at 50 °C for 20 min. The residue was resuspended with 6 mL isopropanol and then vortexed for ten seconds. In addition, an empty vial was added 1.5 mL of isopropanol for quality control of the blank sample.

3.7 UHPLC-MS settings

3.7.1 UHPLC configurations

Chromatographic separation of lipids was performed on a Waters Acquity UPLC instrument (Waters, Milford, MA, USA), equipped with a Waters Acquity Premier C18 reverse phase column (2.1 mm x 100 mm, 1.7 μm particle size, Waters, Milford, MA, USA). The gradient elution program (Table 4/Figure 16) consisted of mobile phase A (50%/50% acetonitrile/MilliQ-water) and mobile phase B (49.5%/49.5% 2-propanol/acetonitrile, 1% MilliQ-water). In addition, each mobile phase contained 1 mM ammonium formate (NH_4FA) and 0.01% formic acid (FA). To avoid precipitation of lipids, the autosampler temperature was set to 20 °C. The column temperature was set to 60 °C. Sample injection volume was 2 μL for each injection, and the flow rate was set to 0.5 ml/min for the entire analysis. Total runtime was 28 min, which included three minutes of equilibration.

Table 4 – Gradient elution program of mobile phase A and B.

Time (min)	%A	%B
0	70	30
15	25	75
20	5	95
25	5	95
25.10	70	30
28	70	30

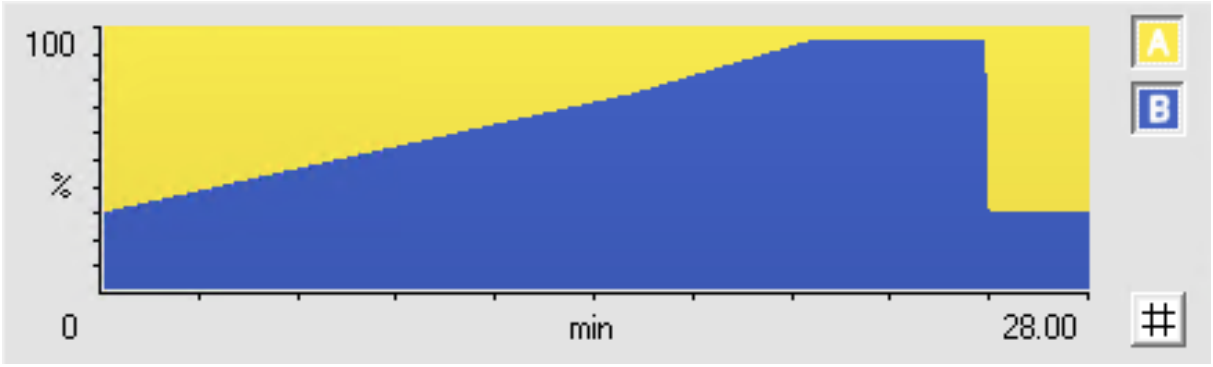

Figure 16 – Gradient elution profile of mobile phases.

3.7.2 MS configurations

MS measurements were obtained using an *Orbitrap ID-X Tribrid MS* (Thermo Fisher Scientific, Waltham, MA, USA). The MS system was coupled to an API configured in H-ESI mode and operated in positive and negative ion mode in two separate analyses. The following ion source parameters were applied; positive ion spray voltage: 3500 V, negative ion spray voltage: 2500 V, sheath gas: 20 arbitrary units (a.u.), auxiliary gas: 10 a.u. and sweep gas: 2 a.u. The capillary- and vaporizer temperatures were set to 350 °C and 400 °C, respectively. RF lens was set to 40%.

3.7.2.1 Full scan

To cover all lipids of interest the *m/z* scan range was chosen from 250 to 1500. Full scan was acquired with MS resolution of 120´000 FWHM (*m/z* 200, default). Orbitrap mass scan (MS OT) performed for the ID-sample was selected as the master scan for further MS^n analysis.

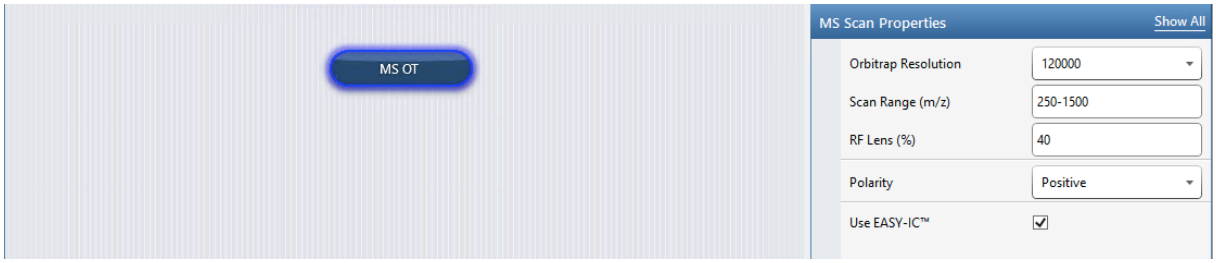

Figure 17 – MS OT was chosen for full scan of ID-samples.

3.7.2.2 MS^n fragmentation

After MS OT, all ions present in the ID-sample with an intensity above a user defined threshold of $1.0e^5$ were isolated in the quadrupole for further HCD-fragmentation ($ddMS^2$ OT HCD). Comprehensive CID MS^2 scans ($ddMS^2$ OT CID) were performed for precursor ions of PC, triggered by targeted mass of the corresponding head group (*m/z* 184.0733) detected from HCD MS^2 data, for total PC lipid identification. Absolute identification of TG required additional CID MS^3 scans ($ddMS^3$ OT CID) triggered by HCD MS^2 product ions due to neutral loss of fatty acid and ammonia (47). MS^n analysis comprised dynamic exclusion, where the precursor ions were put into an exclusion list for four seconds after fragmentation. In addition, targeted mass exclusion ensured in-depth fragmentation, by continuously updating an exclusion list for the ID-samples (Figure 18). MS^n fragmentation parameters can be seen in Appendix 1. MS^n measurements were performed in cycles of 1.5 seconds.

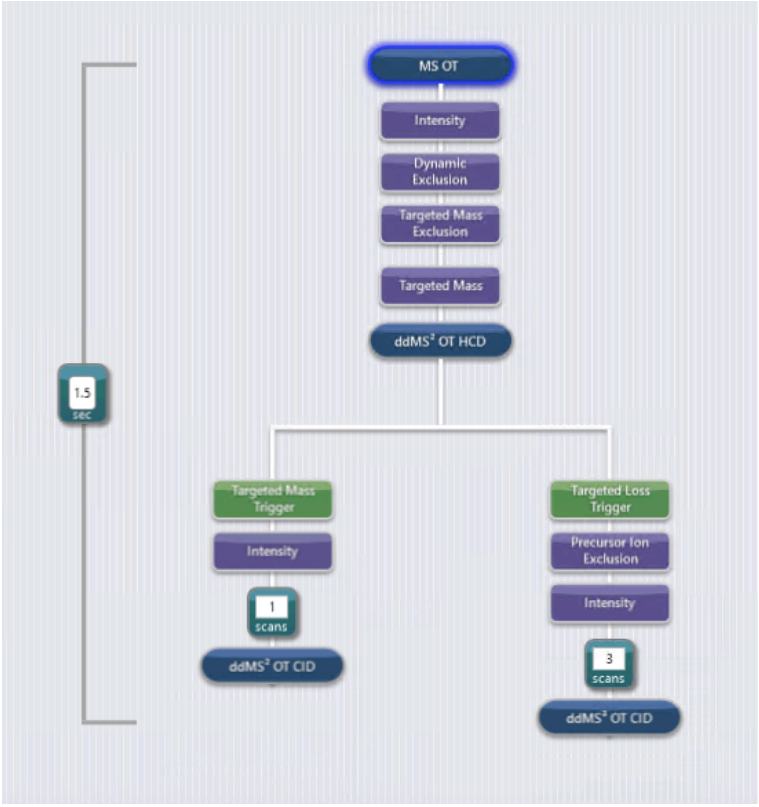

Figure 18 – MS workflow in cycles of 1.5 seconds for lipid profiling. $ddMS^2$ OT CID is triggered by a targeted mass. $ddMS^3$ OT CID is triggered by a targeted loss.

3.8 Acquisition workflow

Data dependent acquisition (DDA) was performed by the AcquireX Data Acquisition Technology (ThermoFisher Scientific, Waltham, MA, USA). The automated acquisition setup was done in deep scan data-dependent mode, but due to software problems with exclusion- and inclusion lists, the acquisition was performed without them. Creation of exclusion lists from fragmented compounds during ID analyses and dynamic exclusion within an analysis worked as normal. The injection sequence started by three injections of the isopropanol-sample and one injection of the blank sample. Further, three replicate injections of an ID-sample were analyzed by MS^n analysis, while triplicate samples from red, blue and white light were injected for full scan. A Qc-sample was also injected for quality control (Table 5). The injection sequence was similar for both positive- and negative ion mode. Altogether, 32 injections with a total runtime of 15 hours were included.

Table 5 – Injection sequence for samples in AcquireX. The same sequence was used for positive- and negative ion mode.

Injection sequence
Isopropanol-sample x 3
Blank
ID-sample x 3
Qc
Red flask x 3
White flask 1 x 3
Blue flask 1 x 3
Qc
White flask 2 x 3
Blue flask 2 x 3
Qc
White flask 3 x 3
Blue flask 3 x 3
Qc

3.9 Data processing

Lipid identification and semi-quantitative analysis were performed by the LipidSearch™ software version 4.2 (ThermoFisher Scientific, Waltham, MA, USA), after importing the raw-files generated in AcquireX. LipidSearch was set to identify lipids species from 19 different lipid classes; MGDG, SQDG, DGDG, DG, MG, TG, LPA, PA, LPC, PC, LPE, PE, LPG, PG, LPI, PI, LPS, PS and ChE in positive and negative ion mode. It was set to identify adducts by hydrogen (H^+), sodium (Na^+) and ammonia (NH_4^+) in positive mode, and de-protonated (H^-) lipids in negative mode. Lipids with a relative standard deviation (RSD) above 20 were rejected, to avoid problems with outliers. Grade A, B, C and D were all applied as ID quality filters, where grade A represented completely identified lipid classes and fatty acids, grade B corresponded to identification of lipid class and some fatty acids, grade C was identification of lipid class or fatty acids, and grade D represented lipid identification by other fragment ions (47). Software conditions for LipidSearch can be seen in Table 6.

Table 6 - LipidSearch parameters

Search Parameter	Settings
mScore	5
RT window	2 min
Intensity threshold	1% of precursor ion
Precursor ion mass tolerance	5 ppm
Product ion mass tolerance	5 ppm

All individual lipid compounds were manually integrated in LipidSearch and the identity was manually checked using Freestyle™ version 1.8 SP1 (ThermoFisher Scientific, Waltham, MA, USA). The dataset was exported to Excel, where relevant data was selected for further analysis in R. In R, parallel values of AUC from the same cultivation conditions were merged into a total AUC representing red light, blue light and white light, respectively. Total AUC values were normalized to 100%, mean and standard deviation (SD) were calculated for each lighting condition. The AUC for each individual lipid was presented as a percentage of total AUC in proportion to its cultivation condition, which is assigned as a percentage of total lipid content (TLC).

In order to investigate the total content of EPA and DHA in each individual lipid, the numbers of 20:5 acyl chains and 22:6 acyl chains were counted and multiplied by the AUC of EPA/DHA in the current lipid. The AUC of EPA/DHA for each individual lipid was presented as a percentage of total AUC of EPA/DHA in proportion to its cultivation condition, which is assigned as a percentage of total lipid content (TLC).

3.10 Statistical analysis

The data of lipid class composition and fatty acid content of DHA and EPA were statistically analyzed using R. Analysis of variance was carried out by an ANOVA test and significance levels were tested by a Tukey HSD post-hoc test. The results are presented as boxplots with mean and plus/minus one SD. SD was calculated based on RSD generated in LipidSearch. The significance level was set to 0.05. Statistical data are included in Appendix 3.

3.11 Identification of SQDG species in *P. glacialis*

Identification of molecular species of SQDG in *P. glacialis* was carried out manually with the FreeStyle software version 1.8 SP1 (ThermoFisher Scientific, Waltham, MA, USA). A library containing fragmentation patterns of different SQDG species was created based on literature search and calculations (13;14;49-56). In Appendix 3, Table 15 holds fragment ions originating from the sulfoquinovosyl head group of SQDG. In Table 16, product ions related to the identification of fatty acyl chains in SQDG are collected. Identification of SQDG was performed in two different ways, one identification method investigated all peaks containing the class-specific product ion, the other identification method investigated molecular ions reported in literature. A criterion for identification of SQDG was that the class-specific product ion at *m/z* 225.0 should be found in the MS^2-spectra. Due to limited time, identifications were only performed for ID-sample one.

4 Results and discussion

4.1 Cultivation and harvesting of *P. glacialis*

Following acclimatization of the *P. glacialis* culture for the conditions of red, blue and white light, the starting concentration for the culture in red light was approximately 50% of the cultures in blue and white light (Figure 19). Low starting concentrations might be a problem, as diatoms may enter a lag phase when subjected to excessive dilution. Nevertheless, a starting concentration of 2.7 x 10^5 cells/L was considered high enough for growth of the culture exposed to red light based on previous experiences from the microalgal researchers at the Norwegian College of Fishery Science.

Diatom cell growth can be measured by counting the numbers of cells per liter or by analyzing the content of the pigment chlorophyll a (Chl a). The growth curves depict a low average growth rate in the culture exposed to red light, compared to blue and white light. These results may indicate that the culture in red light entered lag phase due to low cell count, which resulted in lower growth compared to the cultures cultivated under blue and white light. In red light, growth was seen from the start of cultivation, but after a while it seems to stop. Several factors, such as light absorption, may have influenced the growth in red light.

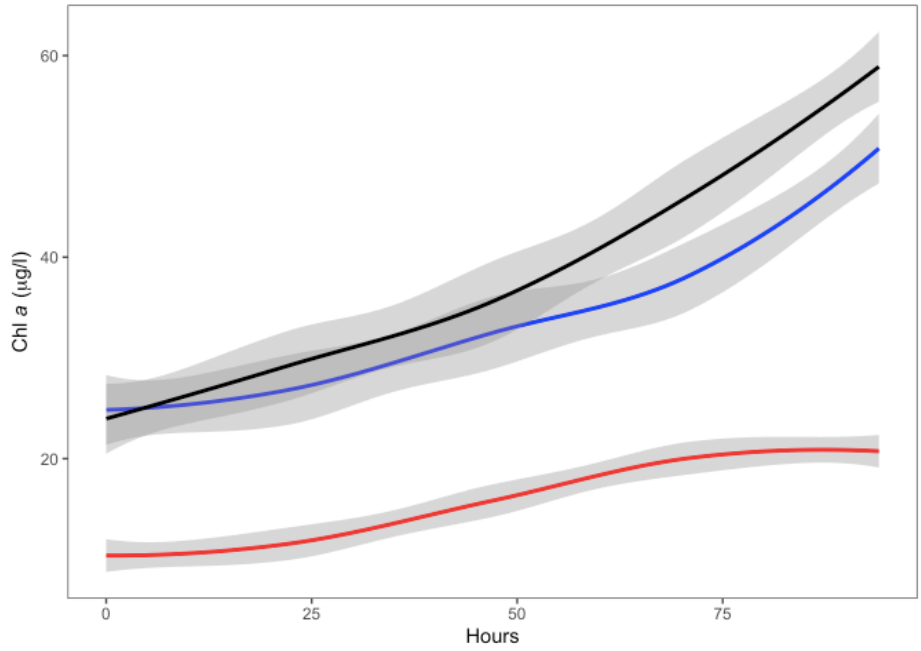

Figure 19 – Average growth rates of *P. glacialis* exposed to red, blue and white light. Shaded error bands: +/- 1 SD.

4.2 UHPLC-MS and analysis of lipids

Prior to the lipid analysis, the total lipid concentration was investigated according to chromatographic quality. Samples were tested with concentrations of 0.05 mg/ml (red), 0.1 mg/ml (dark blue), 0.5 mg/ml (light blue) and 1.0 mg/ml (green), shown in Figure 20. As seen in the figure, the concentration of 1.0 mg/ml had highest signal intensity as expected. The peak was narrow and uniform, thus the chromatographic quality for this sample concentration was considered as good. Higher concentrations than 1.0 mg/ml were not tested, which may be considered for further analysis to optimize the sample concentration of the microalgae culture.

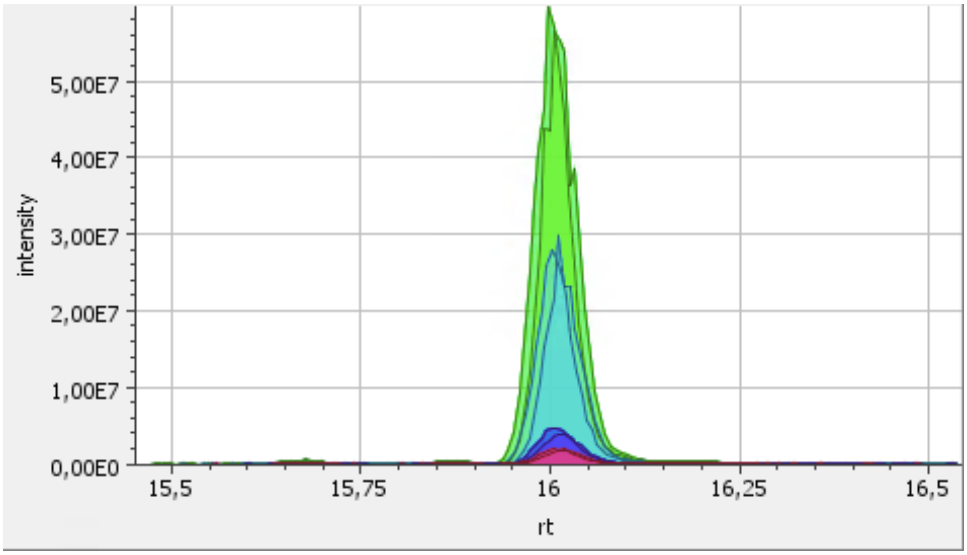

Figure 20 – TG 20:5 12:3 20:5 detected with four different sample concentrations. Red = 0.05 mg/ml, dark blue = 0.1 mg/ml, light blue = 0.5 mg/ml and green = 1.0 mg/ml.

4.3 Lipid class composition

A total of eleven different lipid classes were identified in *P. glacialis* by LipidSearch operating in positive ionization mode. Figure 21 represents the lipid class profile in *P. glacialis* for cultures exposed to red, white and blue light. Apparently, the most abundant lipid class was PC, followed by MGDG, DG and TG, respectively. However, the results are presented with some uncertainty due to the possibility of unequal ionization efficiency for the different lipid classes, which might affect the MS results.

Some variances are seen for the parallels of white and blue light, which is expected for replicates of biological material. Even though the cultivation conditions were similar for all replicates, several factors may influence the environment and growth to some extent. This phenomenon is called bottle effects and may come from small variances in such as temperature, pH or nutrition.

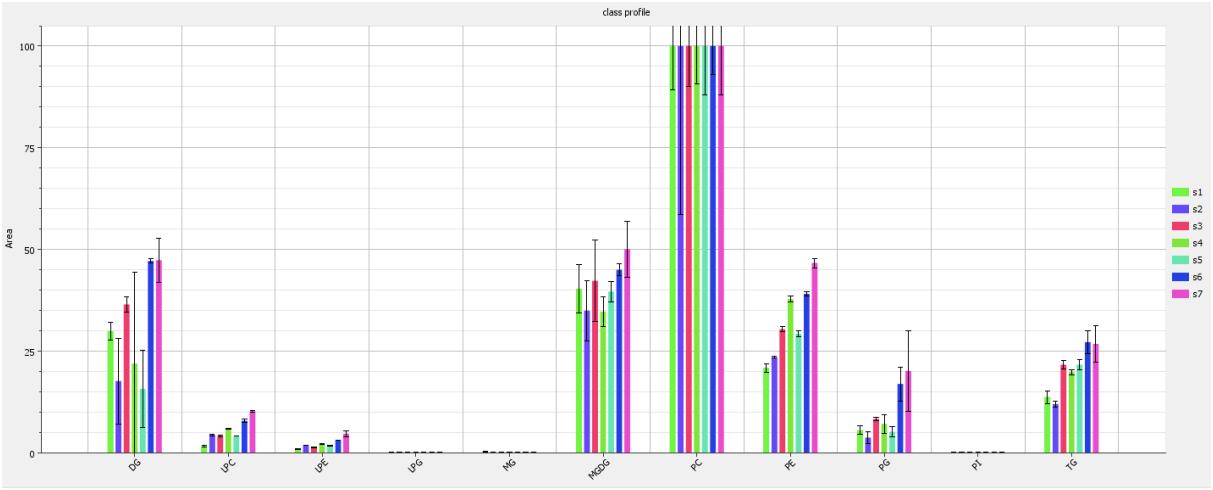

Figure 21 – Histogram with error bars for the lipid class profile of *P. glacialis* in red, blue and white light investigated by LipidSearch in positive ion mode. S1 represents red light, S2-S4 represents white light and S5-S7 represents blue light.

LipidSearch operating in negative ionization mode managed to identify eight different lipid classes (Figure 22). The lipid class SQDG was not identified by the software. The negative ionization results confirm that ionization efficiency strongly influence the signal intensity as in negative mode the signal of PG is most prominent and higher than MGDG, whereas PC is not presented at all, which is opposite of what was seen for positive ionization results. Whit this in mind, precautions should be taken when comparing the amounts of the different lipid classes based on signal intensity of the classes. Due to limited time, lipid composition and fatty acid content for negatively charged lipids were not further investigated. However, this would be interesting for further studies.

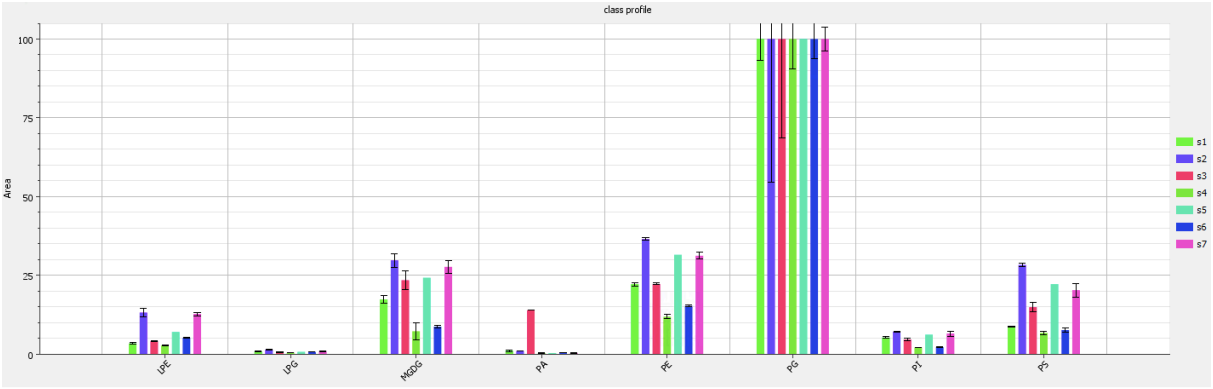

Figure 22 - Histogram with error bars for the lipid class profile of *P. glacialis* in red, blue and white light investigated by LipidSearch in negative ion mode. S1 represents red light, S2-S4 represents white light and S5-S7 represents blue light.

In Figure 23, the lipid class composition of *P. glacialis* is shown as boxplots. Total AUC of lipid content is normalized to 100% for each lighting condition and identified lipid classes are presented relative to this. In the culture exposed to blue light, the content of LPC, LPE and PE were higher than for red and white light ($p < 0.05$). LPC and LPE show similar results, with higher content in blue light compared to white light, and higher content in white light compared to red light ($p < 0.05$). The LPC content in blue light was ~140% higher than in red light, and the LPE content was ~107% higher in blue light compared to red light. Blue light also showed significantly higher proportions of PE than the red and white lighting conditions.

The MG content in red light was remarkable different from the content in blue light, with red light having ~260% higher MG content than blue light ($p < 0.05$). The culture exposed to white light showed a significantly difference in MG content compared to the culture exposed to blue light. Similarly, DG showed significantly highest content in red light, and higher content in white light than in blue light ($p < 0.05$). Among the acylglycerols, TG deviate from the others with almost equal content in red and blue light, significantly higher than in white light.

MGDG also show a significant difference in lipid content for the culture exposed to red light compared to the similar and lower contents in blue and white light. The MGDG content in red light was ~50% higher than in the culture exposed to blue light. The same trend is seen for LPG, with similar content in blue and white light, and a significant difference to red light which had the highest LPG content. The boxplot of PI and PG share the same pattern, with significantly higher content in red light compared to blue and white light with similar content of PI and PG.

PC is presented with significantly higher lipid content in the cultures exposed to white light (≈55%) and blue light (≈54.5%) compared to the culture exposed to red light (≈43%). Even though, the difference between white and blue light is not statistically significant.

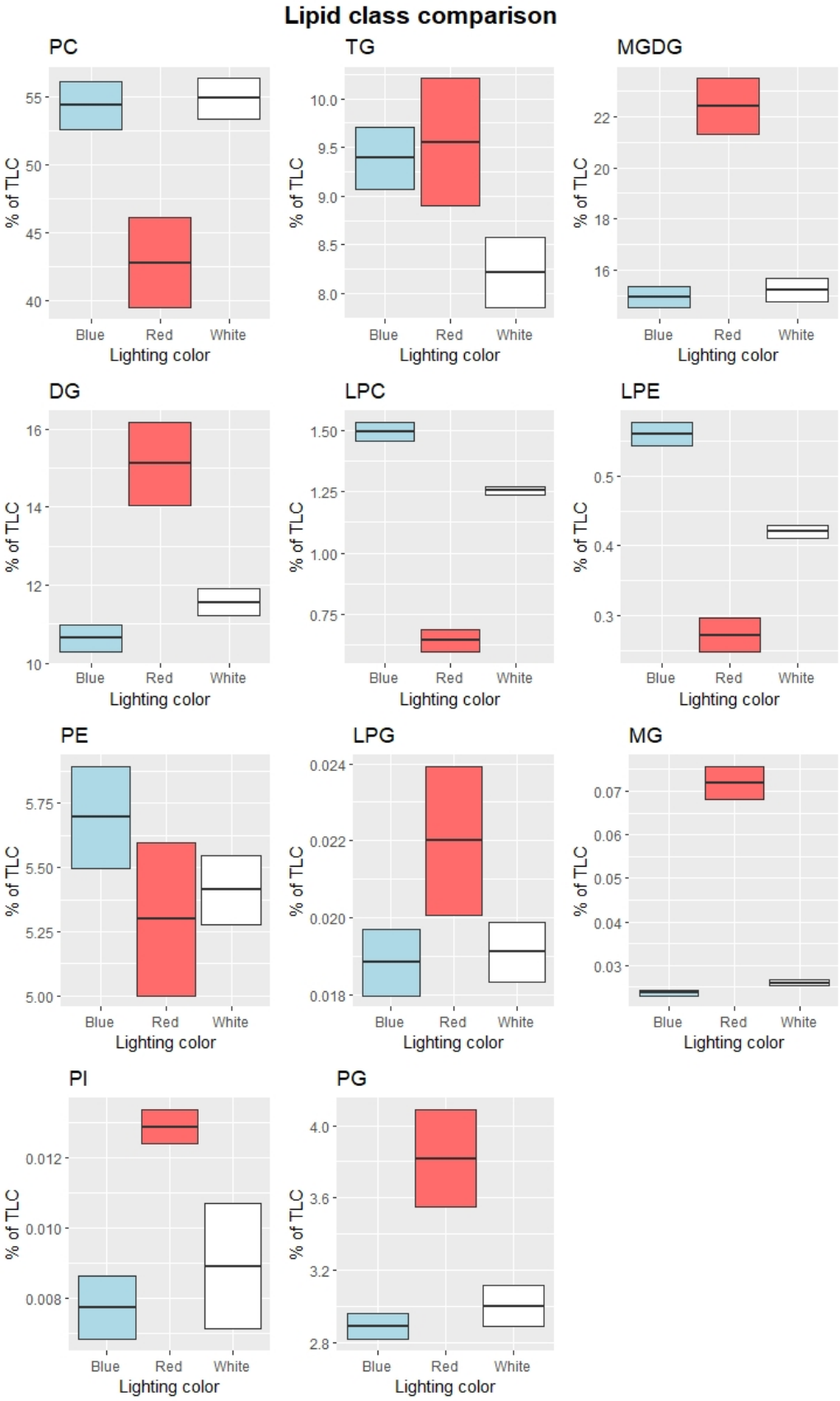

Figure 23 – Boxplot of lipid classes in *P. glacialis* and comparisons of lipid content in red, blue and white light. Boxplots present mean values +/- 1 SD. TLC: total lipid content, presented as the relative AUC in each lipid class relative to total AUC.

It is already known that the lipid composition in diatoms changes relative to their growth phases. A previous master thesis by Myhre investigated lipid composition and fatty acid content in *P. glacialis* when harvested after seven days of cultivation. Myhre observed highest proportion of TG before PC, MGDG and DG, he also reported incidences of TG accumulation (10). In the present study, the cultures were harvested after four days of cultivation, and higher proportion of PC was seen before MGDG, DG and TG. It is known that TG is the main storage lipid in diatoms and that the lipid composition shifts towards higher TG contents in their stationary growth phase, these findings might seem consistent with the literature.

The aquaculture industry requires high quantity of marine lipids for supplement to marine raw materials. Considering this, the study was performed in environments as an approach for production in industrial scale. Investigation of the largest lipid classes in *P. glacialis* show highest lipid content of PC in blue and white light, highest lipid content of MGDG and DG in red light, whereas TG was found with highest lipid content in blue and red light. In the study by Myhre, the same trend was seen. TG which was the most prominent lipid class showed significantly higher content in white light compared to red light, although no significant finding between white and blue lighting condition and between blue and red light. For PC, higher content was seen in red and blue light. MGDG and DG were found with highest content in red light by Myhre, which was the same as for the present study.

For some of the smaller lipid classes, large differences were seen between the different light regimes. Both LPC and LPE were seen with significantly higher lipid content in blue light compared to white and red light, and a remarkable higher lipid content was seen in red light for MG compared to blue and white light. Even though the differences are clear for these lipid classes, the results should be seen in a perspective of aquaculture industry where high quantities are required.

However, the results from both studies show that it is rather unclear which light environment is favorable to maximize the lipid content. For the present study, a suggestion might be the lighting conditions of blue and white light as PC comprise to approximately 55% of the total lipid content in these light regimes.

4.4 Fatty acid distribution of lipids

Distribution of EPA (20:5) in different lipid classes in *P. glacialis* can be seen in Figure 24. The boxplot showing overall content of EPA in blue light (≈31.5%), white light (≈31.2%) and red light (≈28%) is presented relative to total lipid content. Large variances are found within each lighting condition, and due to overlap in SD, no significant differences were found between them. Highest content of EPA was observed in PC (~20-24%), PE (~2.55-2.83%) and MGDG (~1.7-2.5%), respectively.

The EPA content in DG, MGDG, PG and LPG were highest for the culture exposed to red light. For these lipid classes, significant differences were observed between red and blue light, and between red and white light. LPC and LPE contained highest EPA content in blue light, white light contained the second highest and red light contained the lowest content of EPA ($p < 0.05$). PC showed similar and highest production of EPA in blue and white light, which was significantly higher than in red light. In TG, the EPA content was higher in blue light compared to red and white light ($p < 0.05$). Large variance and overlap in SD were observed for PE, with no significant differences between the different lighting colors. EPA was not observed in PI and MG.

Compared to the study by Myhre, the overall EPA content in different lighting conditions apparently show a similar distribution between the different lights. With a closer look at the statistics, the EPA content in blue light is significantly higher than in white light and the EPA content in white light is significantly higher than in red light in the study by Myhre (10). As mentioned, the findings were not significant in the present study, which may indicate an even distribution of EPA in the different lighting conditions. Myhre also reports higher overall EPA content in blue (≈52%), white (≈48%) and red light (≈45%) compared to the present study.

As PC constitutes the highest proportion of the total lipid content in *P. glacialis* in this study, it was expected to find high EPA content in PC compared to the other lipid classes. Interestingly, PE proved to contain the highest content of EPA after PC and before MGDG. In the lipid class composition in Figure 23, PE is ranked with fifth highest lipid proportion of the total lipid content while MGDG is ranked with second highest proportion. In the study by Myhre, the highest EPA content was observed in the lipid class of PC, closely followed by TG (10). PC was reported to apparently be the second most abundant lipid class after TG, thus expected a higher content of EPA in TG than in PC.

Observation of the major lipid classes containing EPA, the study by Myhre showed higher content of EPA in blue light for PC and higher content of EPA in both blue and white light for TG. However, the EPA content was higher in red light compared to white light for PC. Similar findings were seen in the present study, where the EPA content in PC dominated in blue and white light. Even though no significant differences were seen between the lighting conditions for the overall content of EPA, the proportion of EPA is remarkably higher in PC compared to the other lipid classes. A suggestion might therefore be to follow the trend of PC, with cultivation in blue and white light to maximize the EPA content in *P. glacialis*.

It should be taken into account that the culture exposed to red light might have been in another growth stage than the cultures exposed to blue and white light. As this might have affected the results, it would have been interesting to reproduce the work and analyzed the lighting distribution for cultures in the same growth phase.

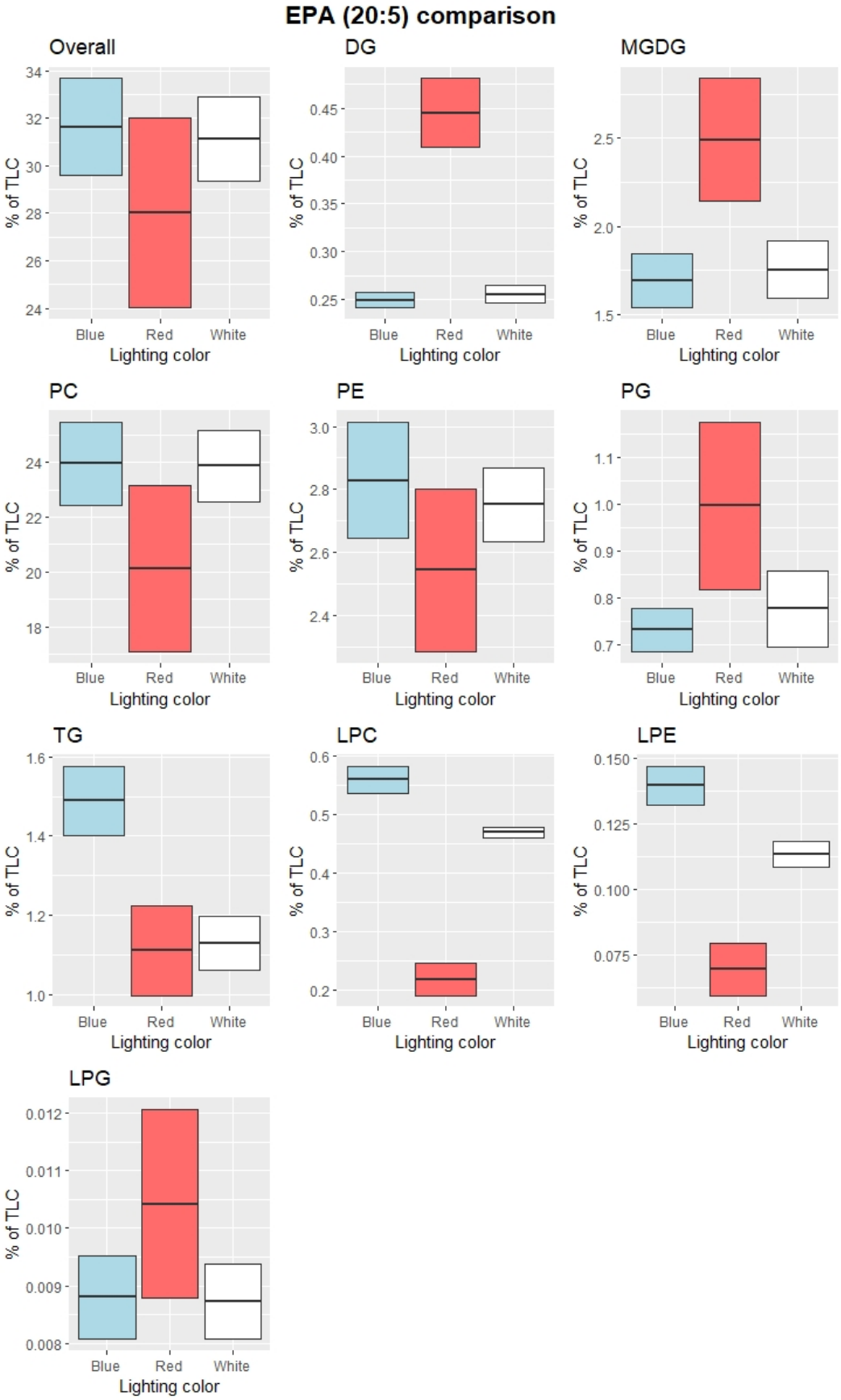

Figure 24 – Boxplot of EPA content in different lipid classes in *P. glacialis.* Boxplots present mean values +/- 1 SD. TLC: total lipid content presented as the relative AUC of EPA in each lipid class relative to total AUC of EPA.

Comparison of DHA (22:6) content in different lipid classes in *P. glacialis* can be seen in Figure 25. A boxplot representing the overall content of DHA, shows highest content of DHA in the culture exposed to red light (3.5%), with a significant difference to blue light (3.0%) ($p \sim 0.02$). DHA content in white light (3.125%) is similar to the content in blue light, and the difference between red and white light is not significant ($p \sim 0.08$). DHA was not observed in LPG, MG and PI.

The DHA content in LPC and LPE were highest in the culture exposed to blue light, with white light having the second highest content of DHA and red light the lowest content ($p < 0.05$). TG and MGDG showed similar distribution of DHA between the different lighting conditions, with large variances in red light which overlaps with the other ($p > 0.05$).

PC contained the highest content of DHA (~1.4-1.8%), which was observed as higher in red and white light compared to blue light. For PE (~0.9-1.11%), DHA content showed to be higher in red and blue light compared to white light ($p < 0.05$). DG and PG share the same trend, with red light as the contributor for highest DHA content, significantly higher than blue and white light.

The results show a considerably lower overall content of DHA (~3-3.5%) compared to the overall content of EPA (~28-31.8%) in *P. glacialis.* This finding was consistent with other studies, showing the fatty acid profile of diatoms being dominated by EPA compared to DHA. A similar finding was also seen for the study by Myhre (10).

Myhre also reported higher percentage of the overall DHA content compared to the present study. As mentioned, Myhre reported higher percentage of the overall EPA content as well. Known that the cultivations were performed in 8 ºC for the study by Myhre and between -1.8 and 5.7 ºC for the present study, investigation of temperature as an effect on fatty acid content was considered. A previous study by Svenning et al. found that the PUFA content remained stable in a temperature range of 2-12 ºC (27). Based on this finding, the suggestion of temperature effect on PUFA content was not validated. As mentioned, the two studies were performed for cultures in different growth phases, which also might influence the overall DHA content.

In the present study the overall DHA content appeared to be significantly higher in red light compared to blue light. Although, it is hard to conclude which lighting condition that contribute to maximize the DHA yield, as the culture in red light is not significantly different from the culture in white light, and the white light is not significantly different from the blue light. Similar as for EPA, the highest contents of DHA were seen in PC and PE, which comprise to the major proportion of DHA content in *P. glacialis*. The highest DHA content is seen in red and white light for PC, whereas for PE the highest DHA content is seen in red and blue light. To compare, Myhre observed the overall content of DHA to be highest for the culture exposed to blue light, the same trend was seen for the largest classes of DHA content, which was TG and PC (10).

Based on findings from the present study, the red lighting condition seem promising in cultivation of P. glacialis for high contents of DHA. However, the contribution from the other lighting conditions should not be excluded.

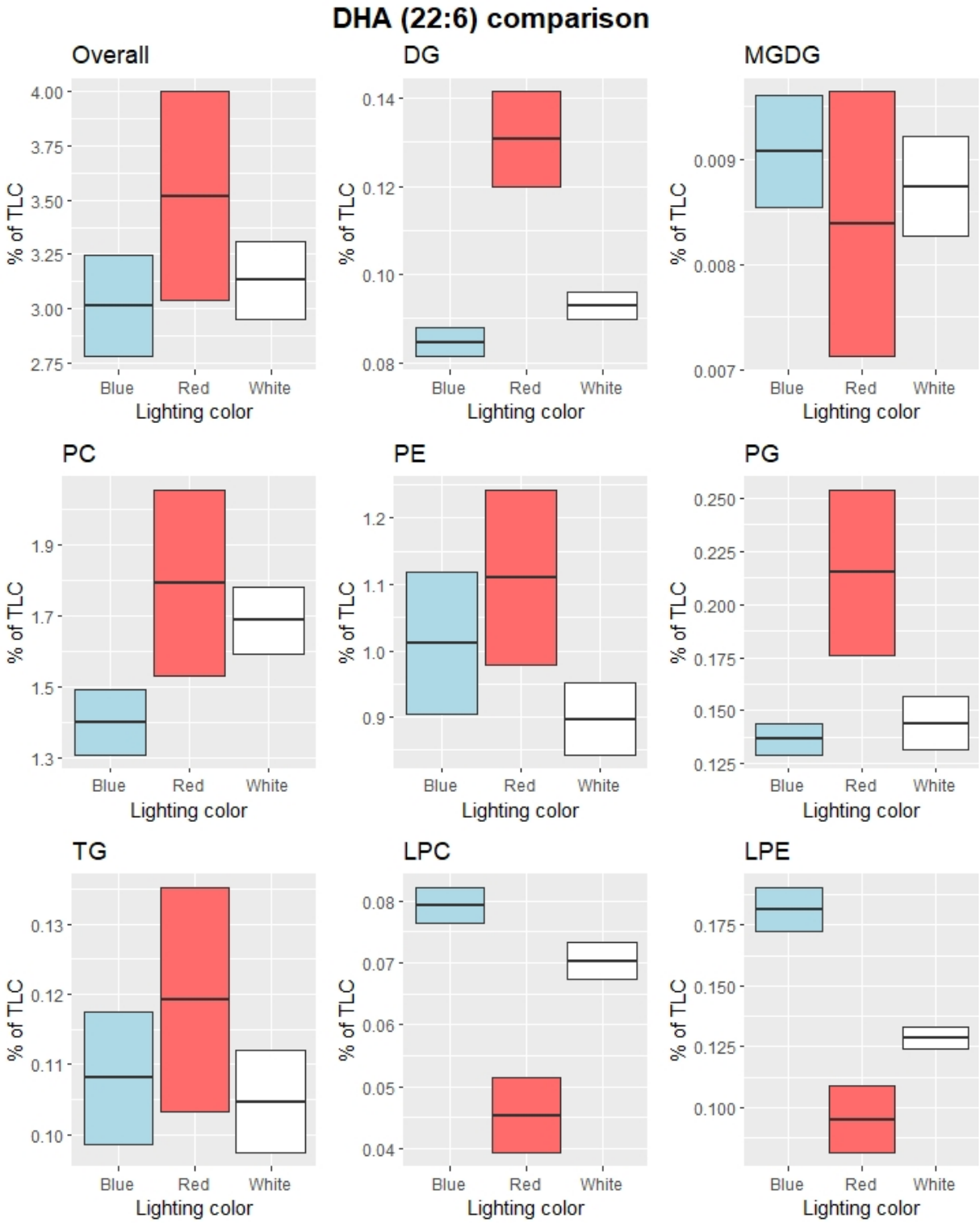

Figure 25 - Boxplot of DHA content in different lipid classes in *P. glacialis.* Boxplots present mean values +/- 1 SD. TLC: total lipid content presented as the relative AUC of DHA in each lipid class relative to total AUC of DHA.

4.5 Validation of method

An overview of the numbers of lipids identified by LipidSearch within each lipid class can be seen in Table 7. LipidSearch managed to identify 225 different lipid species. Of these, ~18% were only presented with fatty acid group key, which only assigns the total number of carbons and double bonds within the fatty acids. This means that detected product ions for these lipids were sufficient for identification of the head group, but insufficient to fully confirm the fatty acyl chains. The intensity threshold at 1% can also filter out product ions enabling detection of fatty acyl chains. A grading system from A to D was used to clarify the identifications. Calculations showed that ~49% of all individual lipids were completely identified by lipid class and fatty acids, whereas in ~51% of all individual lipid identifications, lipid class and/or fatty acids were not fully verified (Grade B-D).

The fatty acid group key leaves several possibilities of fatty acyl chain combinations for the respective lipid species. For DG and PC, 40% and ~38% of all lipids were not identified by fatty acids, which leaves a possibility for EPA and DHA being some of them. Due to insufficient identification by LipidSearch, it is possible that some of the EPA and DHA content may be missing, which in turn may affect the results.

Table 7 – Overview of the numbers of lipids identified in each lipid class by LipidSearch, the corresponding grading system (A-D) and the numbers of lipids presented by fatty acid group key.

Lipid class	Numbers of lipids	Fatty acid group key	Grade A	Grade B	Grade C	Grade D
DG	25	10	12	3	10	
PC	45	17	17	11	17	
MG	2				2	
TG	68	2	52	14	2	
MGDG	32	2	10	20		2
PI	2		2			
LPC	7			7		
LPE	4			4		
PE	23	5	11	7	5	
PG	15	4	7	4	4	
LPG	2			2		
Total	225	40	111	72	40	2

Identification by LipidSearch involve integration of AUC for each sample implemented. Incomplete integration was observed for several lipid compounds, due to problems with the software finding an appropriate cutoff for all samples included in the run. Manual integration was therefore required to assure that the integration was done the same way for all compounds.

For some lipid species, the chromatographic peak was partially outside the retention time window automatically set by LipidSearch (Figure 26). A problem with this is that the AUC will not represent the total area of the peak. If some samples are partly integrated whereas others are fully integrated, it may affect the distribution between samples, which in turn may affect the total AUC and lead to high values for SD. Compounds exposed to this were therefore manually rejected in LipidSearch.

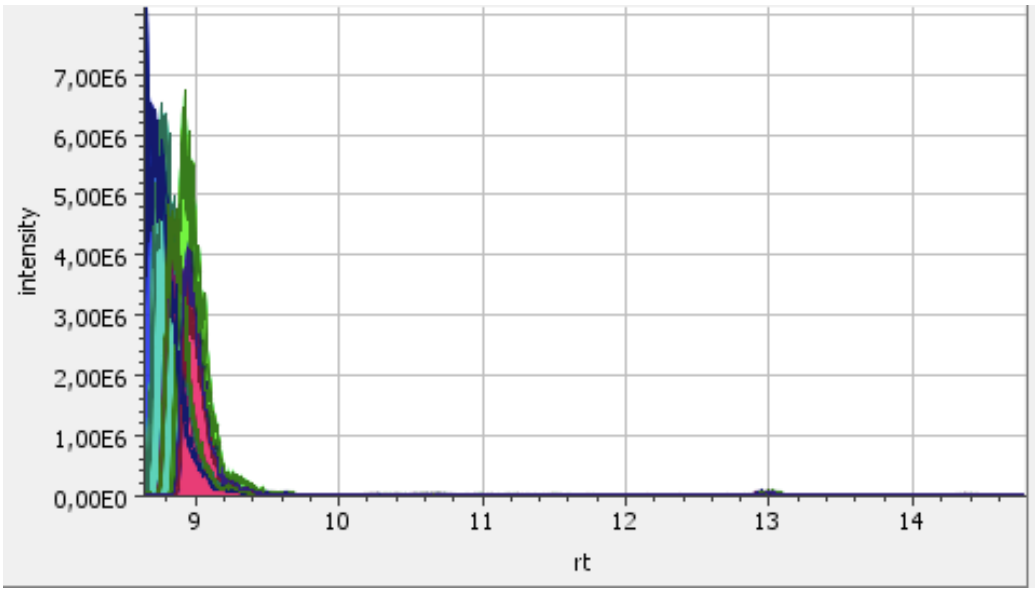

Figure 26 – Incomplete integration in LipidSearch of PG 36:6.

4.6 Identification of molecular species of SQDG in *P. glacialis*

Since *P. glaicialis* belongs to the family of diatoms, a photosynthetic group of microalgae, it was of interest to investigate the occurrence of SQDG which is a primary constituent of the thylakoid membrane. A sulfonic acid in the sulfoquinovosyl head group, makes SQDG mainly ionizable in negative mode and primarily detectable as $[M-H]^-$ ions. LipidSearch version 4.2 was of great benefit for identifications in positive mode, some classes were also identified in negative mode, but SQDG could not be identified. Manual inspection of SQDG in *P. glacialis* was therefore performed in FreeStyle.

Analysis of molecular species of SQDG in *P. glacialis* was performed by UPLC-MS measurements of three parallel ID-samples. The chromatogram in Figure 27 shows all detected signals of the *m/z* 225.0 product ion, in the first ID-sample. Two molecular species of SQDG were identified for the peaks with retention time 5.12 min and 6.61 min.

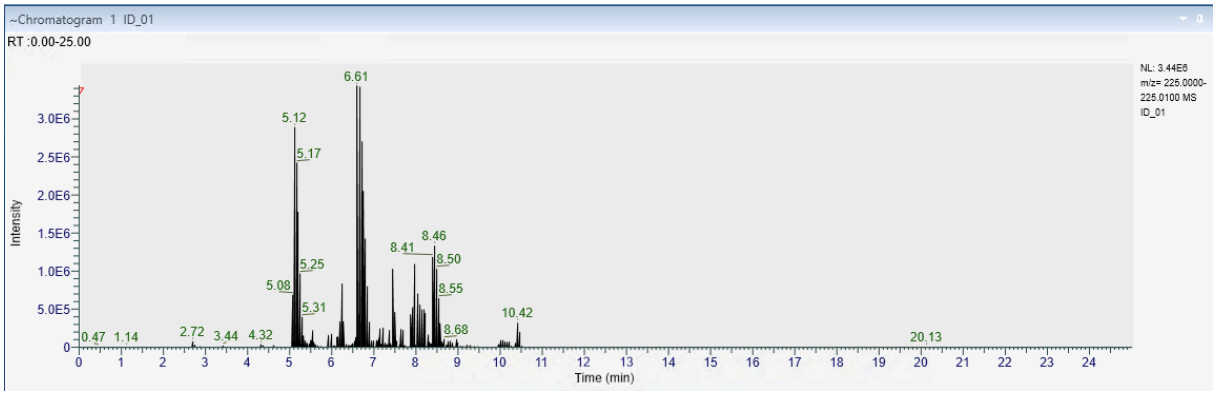

Figure 27 - Chromatogram of the detected class-characteristic product ion at *m/z* 225.0 in ID-sample one. SQDG 14:0 16:4 and SQDG 14:0 18:4 were identified in the peaks with retention time 5.12 min and 6.61 min, respectively.

Due to limitations in time, the other peaks in this chromatogram were not investigated. Presumably, there may be identified several more molecular species of SQDG for the most intense peaks in this chromatogram. Comparison between the three chromatograms of the ID-samples show much of the same peaks. When investigated, the peaks from ID-sample two and ID-sample three were seen as isotopes of the molecular species found in ID-sample one (Figure 28 and 29). These results indicate that the ID-samples consists of a limited number of SQDG with high intensity, although there may be far more with lower intensity. The peaks with retention times 5.12 min and 6.63 min are found in all chromatograms. Further investigations confirmed the presence of the C^{13}-isotope in both peaks in both ID-samples, which may explain

the similarities between the chromatograms. The C^{13}-isotope was also found in some of the adducts of these peaks, which are discussed later.

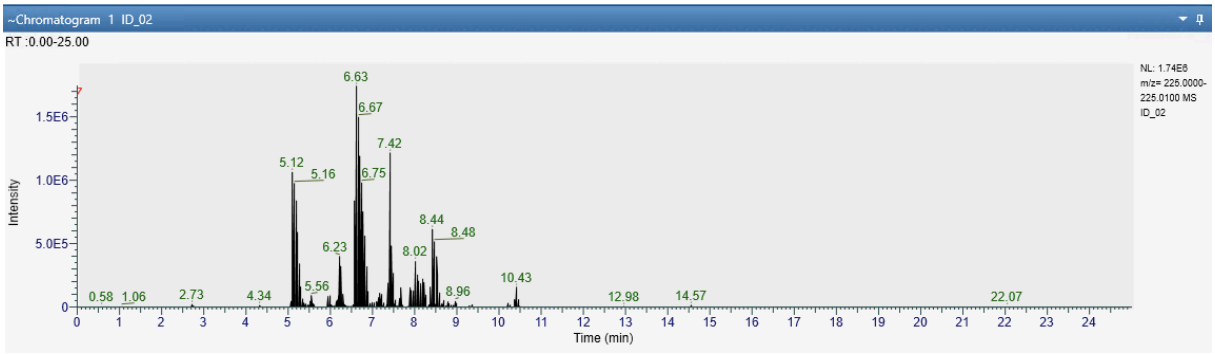

Figure 28 – Chromatogram of the detected class-characteristic product ion at *m/z* 225.0 in ID-sample two.

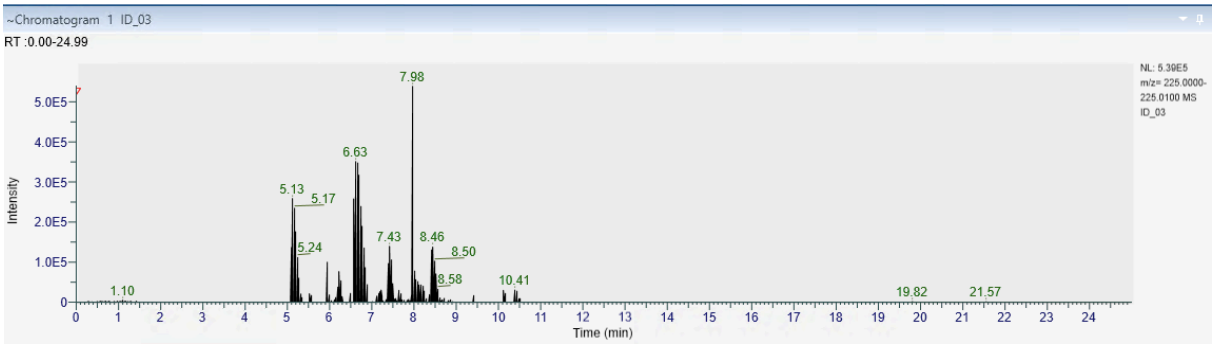

Figure 29 – Chromatogram of the detected class-characteristic product ion at *m/z* 225.0 in ID-sample three.

In Figure 27, the peak with retention time 5.12 min was inspected for three different precursor ions containing the class-diagnostic product ion at *m/z* 225.0 in their fragmentation pattern. Comparisons between the chromatograms of the three precursor ions and the chromatogram of *m/z* 225.0 can be seen in Figure 30. These chromatograms correlate with the same peak width, peak shape and fragmentation pattern, assigning the presence of the same SQDG species.

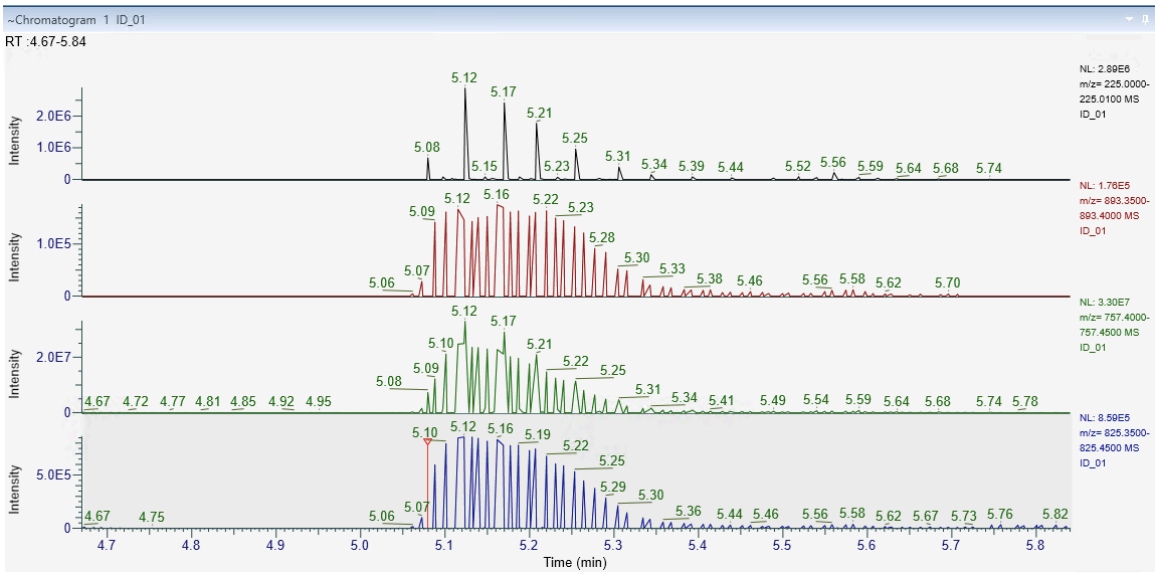

Figure 30 – Chromatogram of *m/z* 225.0 at the top and the chromatograms of the precursor ions at *m/z* 893.39, 757.42 and 825.40. Correlation is seen between all chromatograms for the peak at 5.12 min.

Table 8 - Fragmentation patterns of correlating precursor ions in the peak at 5.12 min, showing the most abundant product ions.

Precursor ion (*m/z*)	Product ions (*m/z*)
757.42	164.9862
	188.9874
	227.2016
	247.1705
	299.0454
	509.2422
	529.2112
	547.2210
825.40	164.9861
	509.2425
	529.2115
	757.4188
893.39	299.0445
	509.2416
	529.2134
	757.4188
	825.3822

The fragmentation patterns of the peak at 5.12 min are listed in Table 8. In the HCD-MS^2 spectra, product ions are observed at *m/z* 164.9862 and *m/z* 299.0454. The literature propose the empirical formulas $[C_4H_5O_5S]^-$ and $[C_9H_{15}O_9S]^-$ for these fragments, which both originates from the sulfoquinovosyl head group (14;53). Together with the class-diagnostic product ion, *m/z* 164.9862 and *m/z* 299.0454 also contributes to the confirmation of a SQDG lipid.

Inspections of the fragmentation patterns interestingly showed *m/z* 757.42 as a product ion of the correlating precursor ions. A mass difference of 67.98 Da was seen between *m/z* 893.39 and 825.40, and between *m/z* 825.40 and 757.42. Kachman et al. reported a mass of 67.9874 as $NaHCO_2$, which was seen as an adduct for LysoPC 16:0 analyzed by RPLC-MS in negative ion mode (57). An explanation might be that *m/z* 757.42 is the molecular ion of SQDG, while *m/z* 893.39 and 825.40 are $NaHCO_2$-adducts. Another observation was that the peak intensity was highest for *m/z* 757.42 compared to the other precursor ions. When investigating the fragmentation patterns for the different precursor ions, fatty acid product ions (discussed later) were only detected for *m/z* 757.42, which also might be an indication for *m/z* 757.42 as the molecular ion (Figure 31).

In the MS^2 spectra in Figure 31, product ions are detected at *m/z* 509.2422 and 529.2112, which correspond to neutral losses of a 16:4 acyl chain ($[M\text{-}H\text{-}C_{15}H_{23}COOH]^-$), and a 14:0 acyl chain ($[M\text{-}H\text{-}C_{13}H_{27}COOH]^-$), respectively. Despite low signal intensity, another product ion was seen at *m/z* 247.1705, which corresponds to the carboxylate anion of a 16:4 fatty acid. A carboxylate anion was also detected for the 14:0 fatty acid, at *m/z* 227.2016. Because of a ten times lower signal intensity for the carboxylate anions compared to the other product ions, these product ions were not visible without zooming in, shown in Figure 32. Molecular species of SQDG may also be identified by neutral losses of aldehyde. A product ion was detected at *m/z* 547.2210 for the same molecular ion, which assign a neutral loss of aldehyde for SQDG containing the 16:4 fatty acyl chain. Based on these fragment ions, the molecular ion at *m/z* 757.42 can be identified as SQDG 14:0 16:4.

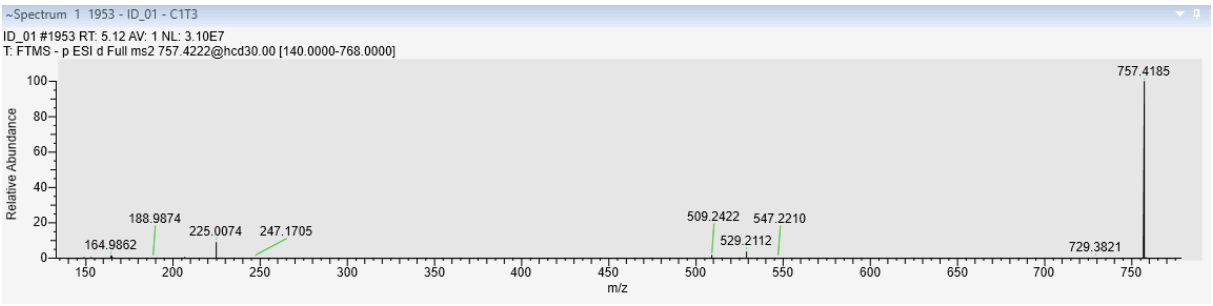

Figure 31 – HCD-MS^2 product ion detection originating from *m/z* 757.4222.

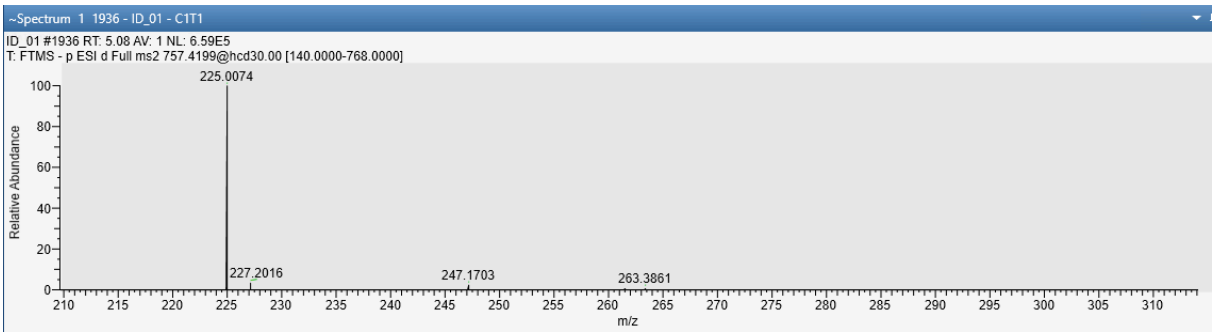

Figure 32 – HCD-MS^2 product ion detection of carboxylate anions at *m/z* 247.1703 (16:4) and 227.2016 (14:0).

In the chromatogram of ID-sample one, a peak was also investigated at 6.61 min with three correlating precursor ions to the peak of *m/z* 225.0 (Figure 33). The corresponding fragmentation patterns can be seen in Table 9. The lipid class was determined by the characteristic *m/z* 225.0 product ion and by *m/z* 164.9860 which corresponds to the $[C_4H_5O_5S]^-$ fragment. As seen for SQDG 14:0 16:4, a mass difference of 67.98 Da is also observed here between *m/z* 921.426 and 853.43, and between *m/z* 853.43 and 785.45, which may indicate the presence of $NaHCO_2$ adducts. Furthermore, *m/z* 785.45 was also in this case shown as the most intense precursor ion, in addition to be an intense product ion in the fragmentation patterns of the other precursor ions. Due to these findings, *m/z* 785.45 is suggested as the molecular ion.

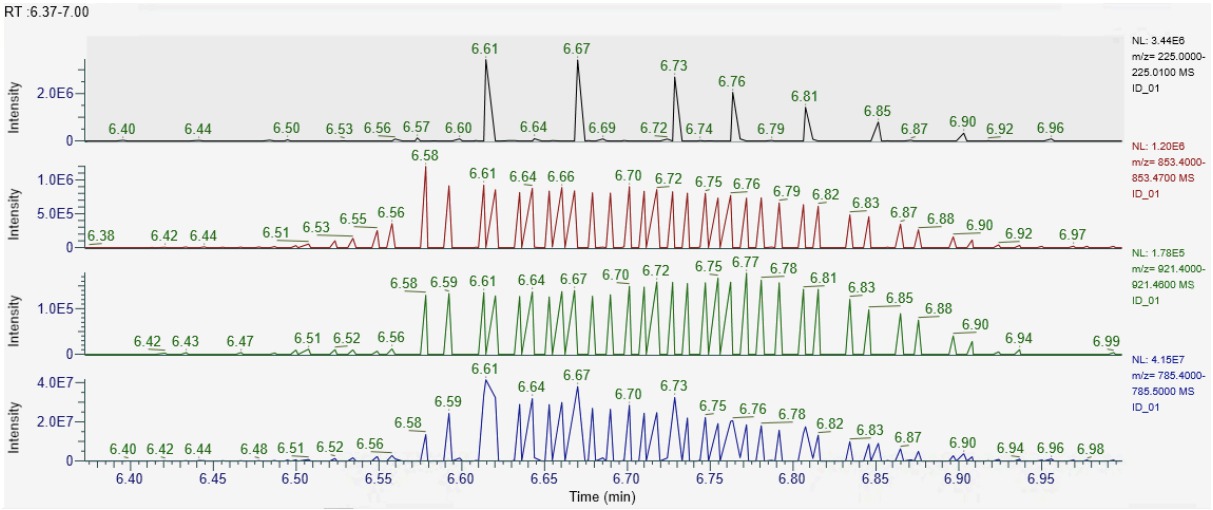

Figure 33 – **Chromatogram of *m/z* 225.0 at the top and the chromatograms of the precursor ions at *m/z* 853.43, 785.45 and 921.426. Correlation is seen between all chromatograms for the peak at 6.61 min.**

For fatty acid identification, five different product ions were detected. Neutral loss of a fatty acid was detected at *m/z* 509.2420 which correspond to the identification of a 14:0 fatty acyl chain. Another product ion was observed at *m/z* 275.2017, which equals to the exact mass of a negatively charged 18:4 fatty acid. A product ion at *m/z* 557.2418 was also seen. This mass assigns the presence of a 18:4 fatty acyl chain due to neutral loss of a fatty acid ([M-H-RCOOH]$^-$). By subtracting *m/z* 557 from *m/z* 785 a mass difference of 228 Da was found, which corresponds to the mass of a neutral 14:0 fatty acid. The carboxylate anion of 14:0 fatty acid was detected by a weak signal at *m/z* 227.2016 (Figure 34). A product ion at m/z 575.2596 was also seen within the fragmentation pattern of *m/z* 785.45. By using an online lipid calculator, this precursor ion also identified 18:4 fatty acid, this time due to a neutral loss of an aldehyde ([M-H-RCHCO]$^-$). A MS^2-spectrum of the molecular ion at *m/z* 785.45 can be seen in Figure 35. The peak with retention time 6.61 min is thereby identified as SQDG 14:0 18:4.

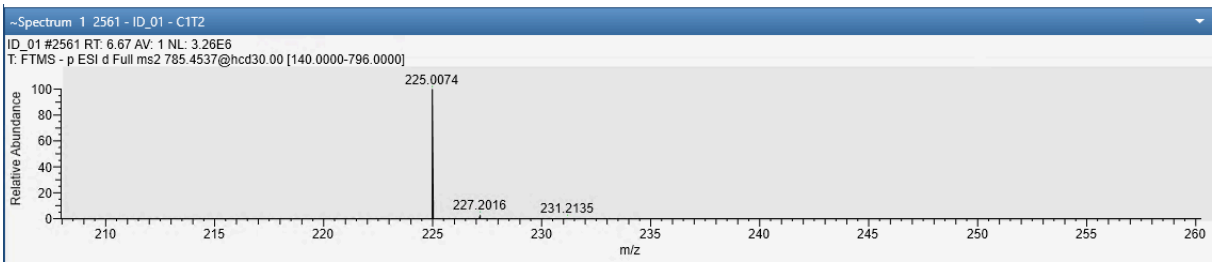

Figure 34 – HCD-MS^2 product ion detection of the carboxylate anion at *m/z* 227.2016 (14:0).

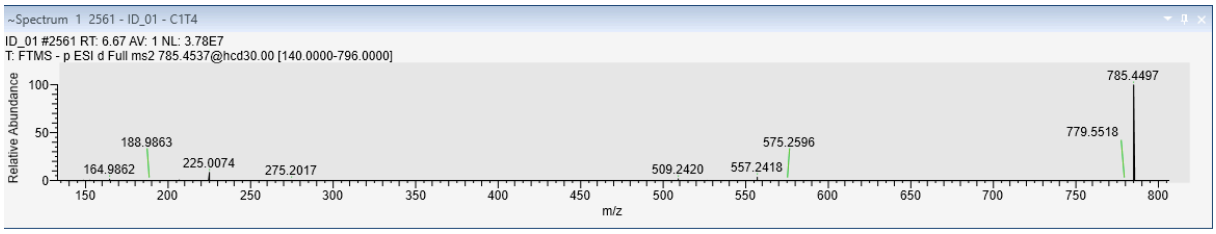

Figure 35 – HCD-MS^2 product ion detection of SQDG 14:0 18:4.

Table 9 - Fragmentation patterns of correlating precursor ions in the peak at 6.61 min, showing the most abundant product ions.

Precursor ion (*m/z*)	**Product ions (*m/z*)**
853.43	164.9860
	509.2427
	557.2421
	785.4514
921.426	299.0434
	509.2425
	557.2411
	785.4514
	853.4260
785.45	164.9862
	188.9863
	227.2016
	275.2017
	509.2420
	557.2418
	575.2596
	779.5518

As recently explained, the method used for identification of SQDG was based on selective detection of the class-specific fragment ion at *m/z* 225.0, with subsequent search for molecular ions and their corresponding fragmentation pattern. Another method was also tested for the purpose of SQDG identification. Prior to the identification, libraries were created for molecular ions and their fragmentation spectra based on literature search. Targeted searches for current molecular ions were performed. To confirm the identity of SQDG molecular species, class-specific fragment ions should be detected in the molecular ion chromatogram. Identity confirmation was divided into three groups, where the simplest confirmation was solely based on the molecular ion and the *m/z* 225.0 fragment. In this case, only fatty acid group key could be assigned. For the two other groups the identity of SQDG was in addition to the m/z 225.0 fragment confirmed by detection of one or two fatty acyl chains. To validate the method, the isolation windows of all identified molecular species were investigated, only finding some interference for SQDG 16:2 16:0 (Appendix 4).

The results from the last method described are presented in Table 10. After investigation of all ID-samples, a total of 19 distinct SQDG species were detected. This method showed to be time consuming, as a lot of time was spent for literature searches. Another disadvantage to this method is that a lot of results may be missed, as the identification is based on a selection of SQDG compounds. As opposed, the first method described basically include all SQDGs present in the sample, which is advantageous when total number of SQDG molecular species is investigated. This first method was also less time consuming. Generally, the method shown in Table 10 may be preferable when identification of specific SQDG species is desired. However, as LipidSearch theoretically includes all possible combinations of fatty acids, manual identification by literature search and theoretical fragments will be unnecessary when the software works as intended.

Table 10 – Identification of SQDG species in *P. glacialis* based on literature search of molecular ions. Identity confirmation of SQDG divided into three different groups: identification of *m/z* 225.0 together with both acyl chains, identification of *m/z* 225.0 together with one acyl chain, identification of *m/z* 225.0 solely.

Identification	$[M - H]^-$ (m/z)	Acyl Chain Composition	Acyl Chain Combination
	737.5	28:00	14:0 14:0
	759.5	30:3	14:0 16:3
Both acyl chains	763.5	30:1	14:0 16:1
and	765.5	30:0	14:0 16:0
m/z 225 fragment ion	789.5	32:2	16:1 16:1
	791.5	32:1	16:0 16:1
	811.5	34:5	20:5 14:0
	839.5	36:5	20:5 16:0
	751.5	29:0	15:0 14:0
	761.5	30:2	14:0 16:2
One acyl chain	785.5	32:4	14:0 18:4
and	789.5	32:2	16:2 16:0
m/z 225 fragment ion	813.5	34:4	16:0 18:4
	811.5	34:5	16:1 18:4
	787.5	32:3	16:3 16:0
	787.5	32:3	14:0 18:3
m/z 225 fragment ion	735.5	28:1	
and	793.5	32:0	
precursor ion	859.5	38:4	

Interestingly, several negatively charged lipid classes are identified by LipidSearch, whereas the sulfolipid SQDG is not being identified by the software. However, the results from manual identification confirm the presence of SQDG in *P. glacialis* by detection of class-specific fragment ions, neutral losses of fatty acids, neutral losses of aldehyde and carboxylate anions. Manual identification is time consuming and not optimal for large datasets of low-abundant lipids. Improvement of the LipidSearch software should therefore be considered, which in return will give valuable information about lipid profiles for negatively charged lipids.

Manual identification of SQDG was performed with the same MS settings and extraction methods as for lipids identified in positive ionization mode, except that the capillary was set to negative voltage resulting in negative ionization. The identifications were performed on a sample containing several different lipid species. As the identification was performed manually, the abundance of SQDG relative to other lipids in the sample is unknown. A suggestion for further analysis may be to do several lipid extractions to ensure an ideal concentration for identification of SQDG. The extraction method of SQDG should also be optimized according to extractants and solvents. The sulfoquinovosyl head group contains a permanently negative charge which should be considered when choosing solvent. Furthermore, SQDG was investigated by HCD-MS^2 analysis, solely. For further analysis, the MS settings should be optimized for the purpose of SQDG identification.

4.7 Limitations of the study

In the lipid class comparison and fatty acid distribution comparison the SD for red light was much higher than for blue and white light. This trend probably comes from a three times lower injection of replicates for red light compared to the two other lighting colors. Ideally, the replication number should have been the same for all groups to improve statistical strength.

The numbers of parallels from red (n=3), blue (n=9) and white light (n=9) were rather low. A higher number of parallels would have been necessary to achieve representative samples from the different cultivation conditions, which is desirable to be able to generalize the results. Furthermore, a higher number of parallels is desirable to improve statistical strength.

The acquisition workflow was not able to run exclusion list. With the absence of an exclusion list, compounds from background interference may be fragmented and analyzed, which results in lesser time for lipid analysis and identification of co-eluting compounds.

Whereas other lipid classes such as PS, PI and MGDG were identified by LipidSearch in negative ionization mode, it is difficult to understand why the software do not manage to identify SQDG, since SQDG is included in the software's list of included lipids. Manually, both class-specific fragment ions and product ions related to the fatty acids are observed, and SQDG species have been identified. However, manual identification is time-consuming and using a functional LipidSearch might have resulted in several SQDG species identifications. Semi-quantitative analysis was therefore not performed for SQDG, neither comparison of EPA/DHA content in SQDG in different cultivation conditions.

5 Conclusion and future perspectives

The aim of the study was to investigate different lighting conditions and their influence on lipid composition and fatty acid content of EPA and DHA in *Porosira glacialis.* The highest content of EPA was observed in PC, with a significantly increased content in the cultures exposed to blue and white light compared to the culture exposed to red light. For the overall content of EPA, an even distribution was seen between the different lighting conditions.

The overall content of DHA was significantly increased in the culture exposed to red light compared to blue light, but not significant between red and white light and between blue and white lighting condition. For the major lipid classes, highest content of DHA was seen in PC for red and white light, and in PE for red and blue light.

The blue and white lighting conditions seem promising to maximize the yield of lipids rich in EPA for *P. glacialis*. However, the findings are not as clear for DHA, but a suggestion might be red light before blue light to maximize the content of DHA. The findings for DHA are not consistent with a previous study by Myhre, where the content of EPA and DHA were significantly highest in blue lighting condition.

Folch extraction and UPLC-MS^2 analysis in negative ionization mode appeared to be sufficient for manual identification of SQDG. Even though other negatively charged lipids were identified by LipidSearch, optimization of the extraction method and the MS method may be required for identification of SQDG by the software. For future work, collaboration with the instrument supplier for software improvement of negatively charged lipids should be prioritized. It would also be interesting to reproduce the work performed in this study to investigate the lipid composition and fatty acid content of EPA and DHA for negatively charged lipids by LipidSearch, which will contribute to a broader understanding of the lipid profile in *P. glacialis*.

Works cited

1. Fiskeoppdrett [web document]. miljodirektoratet.no [updated 2021; cited 6. January 2022]. Available from: https://miljostatus.miljodirektoratet.no/tema/hav-og-kyst/fiskeoppdrett/
2. Tall og fakta om internasjonal handel og samarbeid [web document]. nho.no [updated 2021; cited 12. January 2022]. Available from: https://www.nho.no/analyse/tall-fakta-internasjonal-handel-samarbeid/
3. Sprague M, Betancor MB, Tocher DR. Microbial and genetically engineered oils as replacements for fish oil in aquaculture feeds. Biotechnol Lett 2017;39(11):1599-609. DOI: 10.1007/s10529-017-2402-6
4. Hva er i fôret til laksen? [web document]. laksefakta.no [updated 2021; cited 6. January 2022]. Available from: https://laksefakta.no/hva-spiser-laksen/hva-er-i-foret-til-laksen/
5. Hansen L. The Weak Sustainability of the Salmon Feed Transition in Norway - A Bioeconomic Case Study. Frontiers in Marine Science 2019;6. DOI: 10.3389/fmars.2019.00764
6. Torstensen BE, Espe M, Sanden M, Stubhaug I, Waagbø R, Hemre GI, et al. Novel production of Atlantic salmon (Salmo salar) protein based on combined replacement of fish meal and fish oil with plant meal and vegetable oil blends. Aquaculture 2008;285(1):193-200. DOI: 10.1016/j.aquaculture.2008.08.025
7. Tacchi L, Secombes CJ, Bickerdike R, Adler MA, Venegas C, Takle H, et al. Transcriptomic and physiological responses to fishmeal substitution with plant proteins in formulated feed in farmed Atlantic salmon (Salmo salar). BMC Genomics 2012;13(1):1-21. DOI: 10.1186/1471-2164-13-363
8. Morais S, Silva T, Cordeiro O, Rodrigues P, Guy DR, Bron JE, et al. Effects of genotype and dietary fish oil replacement with vegetable oil on the intestinal transcriptome and proteome of Atlantic salmon (Salmo salar). BMC Genomics 2012;13(1):448-. DOI: 10.1186/1471-2164-13-448
9. De Santis C, Bartie KL, Olsen RE, Taggart JB, Tocher DR. Nutrigenomic profiling of transcriptional processes affected in liver and distal intestine in response to a soybean meal-induced nutritional stress in Atlantic salmon (Salmo salar). Comp Biochem Physiol Part D Genomics Proteomics 2015;15:1-11. DOI: 10.1016/j.cbd.2015.04.001
10. Myhre TN. Lipidomics of marine microalgae with industrial potential [unpublished]. 2021.
11. Christie W. Lipids in Action - Their Biological Functions [web document]. lipidmaps.org [cited 16. December 2021]. Available from: https://www.lipidmaps.org/resources/lipidweb/index.php?page=lipids/basics/whatdo/index.htm
12. Heipieper HJ, Meinhardt F, Segura A. The cis–trans isomerase of unsaturated fatty acids in Pseudomonas and Vibrio: biochemistry, molecular biology and physiological function of a unique stress adaptive mechanism. FEMS Microbiol Lett 2003;229(1):1-7. DOI: 10.1016/S0378-1097(03)00792-4
13. da Costa E, Silva J, Mendonça SH, Abreu MH, Domingues MR. Lipidomic Approaches towards Deciphering Glycolipids from Microalgae as a Reservoir of Bioactive Lipids. Mar Drugs 2016;14(5):101. DOI: 10.3390/md14050101
14. Granafei S, Losito I, Palmisano F, Cataldi TRI. Unambiguous regiochemical assignment of sulfoquinovosyl mono - and diacylglycerols in parsley and spinach leaves by liquid chromatography/electrospray ionization sequential mass spectrometry assisted by regioselective enzymatic hydrolysis. Rapid Commun Mass Spectrom 2017;31(18):1499-509. DOI: 10.1002/rcm.7928

15. Nakajima Y, Umena Y, Nagao R, Endo K, Kobayashi K, Akita F, et al. Thylakoid membrane lipid sulfoquinovosyl-diacylglycerol (SQDG) is required for full functioning of photosystem II in Thermosynechococcus elongatus. J Biol Chem 2018;293(38):14786-97. DOI: 10.1074/jbc.RA118.004304
16. Alagawany M, Elnesr SS, Farag MR, El-Sabrout K, Alqaisi O, Dawood MAO, et al. Nutritional significance and health benefits of omega-3,-6 and-9 fatty acids in animals. Anim Biotechnol 2020:1-13. DOI: 10.1080/10495398.2020.1869562
17. Ferrier DR. Biochemistry. 7. ed. Philadelphia Wolters Kluwer 2017.
18. Simopoulos AP. Evolutionary aspects of diet, the omega-6/omega-3 ratio and genetic variation: nutritional implications for chronic diseases. Biomed Pharmacother 2006;60(9):502-7. DOI: 10.1016/j.biopha.2006.07.080
19. Valenzuela J, Mazurie A, Carlson RP, Gerlach R, Cooksey KE, Peyton BM, et al. Potential role of multiple carbon fixation pathways during lipid accumulation in Phaeodactylum tricornutum. Biotechnol Biofuels 2012;5(1):40-. DOI: 10.1186/1754-6834-5-40
20. Throndsen J, Hasle GR, Tangen K. Norsk kystplankton flora. Oslo: Almater Forlag; 2003.
21. Townsend DW. Oceanography and Marine Biology. Sunderland: Sinauer Associates; 2012.
22. Nguyen H, Fauci L. Hydrodynamics of diatom chains and semiflexible fibres. J R Soc Interface 2014;11(96):20140314-. DOI: 10.1098/rsif.2014.0314
23. Iglikowska A, Krzemińska M, Renaud PE, Berge J, Hop H, Kukliński P. Summer and winter MgCO3 levels in the skeletons of Arctic bryozoans. Marine environmental research 2020;162:105166-. DOI: 10.1016/j.marenvres.2020.105166
24. Orefice I, Musella M, Smerilli A, Sansone C, Chandrasekaran R, Corato F, et al. Role of nutrient concentrations and water movement on diatom's productivity in culture. Sci Rep 2019;9(1):1479-. DOI: 10.1038/s41598-018-37611-6
25. Kallqvist T. Algekulturteknologi - naturgitte forutsetninger og praktiske løsninger. Norsk vannforening; 1999. Vann på nett. Available from: https://vannforeningen.no/wp-content/uploads/2015/06/1999_30723.pdf
26. Kim S-K. Handbook of marine microalgae : biotechnology advances. Amsterdam, Netherlands: Academic Press; [cited].
27. Svenning JB. Towards mass cultivation of diatoms as a source of marine lipids. UiT The Arctic University of Norway; 2021.
28. Yatipanthalawa B, Li W, Hill DRA, Trifunovic Z, Ashokkumar M, Scales PJ, et al. Interplay between interfacial behaviour, cell structure and shear enables biphasic lipid extraction from whole diatom cells (Navicula sp.). J Colloid Interface Sci 2021;589:65-76. DOI: 10.1016/j.jcis.2020.12.056
29. Otero P, Saha SK, Gushin JM, Moane S, Barron J, Murray P. Identification of optimum fatty acid extraction methods for two different microalgae Phaeodactylum tricornutum and Haematococcus pluvialis for food and biodiesel applications. Anal Bioanal Chem 2017;409(19):4659-67. DOI: 10.1007/s00216-017-0412-9
30. Folch J, Lees M, Sloane Stanley GH. A simple method for the isolation and purification of total lipides from animal tissues. J Biol Chem 1957;226(1):497-509. DOI: 10.1016/S0021-9258(18)64849-5
31. Svenning JB, Dalheim L, Vasskog T, Matricon L, Vang B, Olsen RL. Lipid yield from the diatom Porosira glacialis is determined by solvent choice and number of extractions, independent of cell disruption. Sci Rep 2020;10(1):22229-. DOI: 10.1038/s41598-020-79269-z

32. Stabell R. Lipider i silderogn: Ekstraksjon med "grønn teknologi": UiT The Arctic University of Norway; 2021.
33. Han X. Lipidomics for studying metabolism. Nat Rev Endocrinol 2016;12(11):668-79. DOI: 10.1038/nrendo.2016.98
34. Holcapek M. Lipidomics. Anal Bioanal Chem 2015;407(17):4971-2. DOI: 10.1007/s00216-015-8740-0
35. Gross RW, Holčapek M. Lipidomics. Anal Chem 2014;86(17):8505-. DOI: 10.1021/ac5027644
36. Hansen SH, Pedersen-Bjergaard S, Rasmussen KE. Introduction to Pharmaceutical Chemical Analysis. West Sussex: Wiley; 2012.
37. Haugan HS. Investigating the Lipid Coverage of the Dried Blood Spot Metabolome using Liquid Chromatography – Mass Spectrometry for Global Metabolomics. 2020.
38. What is mass spectrometry? [web document]. broadinstitute.org [cited 17. February 2022]. Available from: https://www.broadinstitute.org/technology-areas/what-mass-spectrometry
39. Hu Q, Noll RJ, Li H, Makarov A, Hardman M, Graham Cooks R. The Orbitrap: a new mass spectrometer. J Mass Spectrom 2005;40(4):430-43. DOI: 10.1002/jms.856
40. Perry RH, Cooks RG, Noll RJ. Orbitrap mass spectrometry: Instrumentation, ion motion and applications. Mass Spectrom Rev 2008;27(6):661-99. DOI: 10.1002/mas.20186
41. Transforming small molecule identification and structure elucidation. In.: thermofisher.com [cited 17. February 2022]. Available from: https://assets.thermofisher.com/TFS-Assets/CMD/Specification-Sheets/ps-65188-orbitrap-id-x-tribrid-ms-ps65188-en.pdf
42. Orbitrap Tribrid Series, Hardware Manual. Waltham, MA: Thermo Fisher Scientific; 2018. 80000-97027.
43. Molecular Dissociation Technology Overview [web document]. thermofisher.com [cited 9. December 2021]. Available from: https://www.thermofisher.com/no/en/home/industrial/mass-spectrometry/mass-spectrometry-learning-center/mass-spectrometry-technology-overview/dissociation-technique-technology-overview.html
44. Makarov A, Denisov E, Kholomeev A, Balschun W, Lange O, Strupat K, et al. Performance Evaluation of a Hybrid Linear Ion Trap/Orbitrap Mass Spectrometer. Anal Chem 2006;78(7):2113-20. DOI: 10.1021/ac0518811
45. Bereman MS, Canterbury JD, Egertson JD, Horner J, Remes PM, Schwartz J, et al. Evaluation of Front-End Higher Energy Collision-Induced Dissociation on a Benchtop Dual-Pressure Linear Ion Trap Mass Spectrometer for Shotgun Proteomics. Anal Chem 2012;84(3):1533-9. DOI: 10.1021/ac203210a
46. LipidSearch Software [web document]. thermofisher.com [cited 9. December 2021]. Available from: https://www.thermofisher.com/order/catalog/product/OPTON-30880
47. Kiyonami R, Peake DAY, Y. Miller,K. . Increased Throughput and Confidence for Lipidomics Profiling Using Comprehensive HCD MS2 and CID MS2/MS3 on a Tribrid Orbitrap Mass Spectrometer. CA, USA and Tokyo, Japan: Thermo Fisher Scientific; 2016. Thermo Fisher Scientific report AN64675-EN 0916S.
48. Automated Identification and Relative Quantitation of Lipids by LC/MS [web document]. thermofisher.com [cited 9. December 2021]. Available from: https://assets.thermofisher.com/TFS-Assets/CMD/brochures/BR-63951-LipidSearch-BR63951-EN.pdf
49. Coniglio D, Bianco M, Ventura G, Calvano CD, Losito I, Cataldi TRI. Lipidomics of the Edible Brown Alga Wakame (Undaria pinnatifida) by Liquid Chromatography

Coupled to Electrospray Ionization and Tandem Mass Spectrometry. Molecules (Basel, Switzerland) 2021;26(15):4480. DOI: 10.3390/molecules26154480
50. da Costa E, Melo T, Moreira ASP, Alves E, Domingues P, Calado R, et al. Decoding bioactive polar lipid profile of the macroalgae Codium tomentosum from a sustainable IMTA system using a lipidomic approach. Algal research (Amsterdam) 2015;12:388-97. DOI: 10.1016/j.algal.2015.09.020
51. Keusgen M, Curtis JM, Thibault P, Walter JA, Windust A, Ayer SW. Sulfoquinovosyl diacylglycerols from the alga Heterosigma carterae. Lipids 1997;32(10):1101-12. DOI: 10.1007/s11745-997-0142-9
52. Yan X, Chen D, Xu J, Zhou C. Profiles of photosynthetic glycerolipids in three strains of Skeletonema determined by UPLC-Q-TOF-MS. Journal of applied phycology 2010;23(2):271-82. DOI: 10.1007/s10811-010-9553-3
53. Zhang X, Fhaner CJ, Ferguson-Miller SM, Reid GE. Evaluation of ion activation strategies and mechanisms for the gas-phase fragmentation of sulfoquinovosyldiacylglycerol lipids from Rhodobacter sphaeroides. Int J Mass Spectrom 2012;316-318:100-7. DOI: 10.1016/j.ijms.2012.01.011
54. Zianni R, Bianco G, Lelario F, Losito I, Palmisano F, Cataldi TRI. Fatty acid neutral losses observed in tandem mass spectrometry with collision-induced dissociation allows regiochemical assignment of sulfoquinovosyl-diacylglycerols. J Mass Spectrom 2013;48(2):205-15. DOI: 10.1002/jms.3149
55. Garrett TA, Schmeitzel JL, Klein JA, Hwang JJ, Schwarz JA. Comparative lipid profiling of the cnidarian Aiptasia pallida and its dinoflagellate symbiont. PLoS One 2013;8(3):e57975-e. DOI: 10.1371/journal.pone.0057975
56. Naumann I, Darsow KH, Walter C, Lange HA, Buchholz R. Identification of sulfoglycolipids from the alga Porphyridium purpureum by matrix-assisted laser desorption/ionisation quadrupole ion trap time-of-flight mass spectrometry. Rapid Commun Mass Spectrom 2007;21(19):3185-92. DOI: 10.1002/rcm.3190
57. Kachman M, Habra H, Duren W, Wigginton J, Sajjakulnukit P, Michailidis G, et al. Deep annotation of untargeted LC-MS metabolomics data with Binner. Bioinformatics 2020;36(6):1801-6. DOI: 10.1093/bioinformatics/btz798
58. Molecular Mass Calculator [Database]. Christoph Gohlke [updated 18. June 2021; cited 7. May 2022]. Available from: https://www.lfd.uci.edu/~gohlke/molmass/

Appendix

Appendix 1: MS method

Table 11 - Neutral loss of fatty acids and ammonia triggering ddMS^3 OT CID.

FA	NL (FA + NH_3)	FA	NL (FA + NH_3)
12:0	217.2042	20:3	323.2824
14:0	245.2355	20:4	321.2668
14:1	243.2198	20:5	319.2511
16:0	273.2668	21:0	343.3450
16:1	271.2511	22:0	357.3607
16:2	269.2355	22:1	355.3450
17:0	287.2824	22:2	353.3294
18:0	301.2981	22:3	351.3137
18:1	299.2824	22:4	349.2981
18:2	297.2668	22:5	347.2824
18:3	295.2511	22:6	345.2668
19:0	315.3137	23:0	371.3763
20:0	329.3294	24:0	385.3920
20:1	327.3137	24:1	383.3763
20:2	325.2981	26:0	413.4233

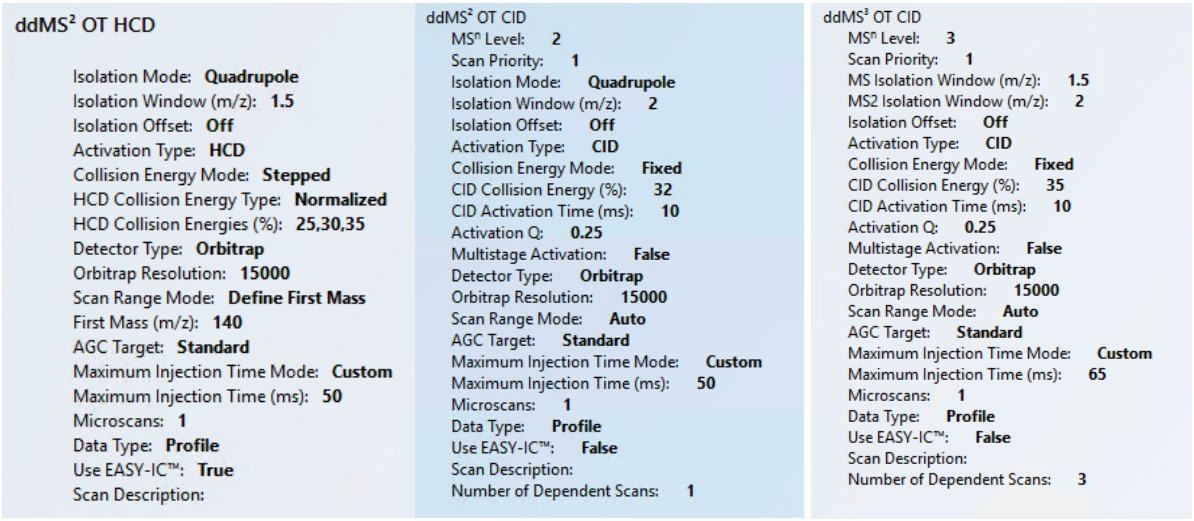

Figure 36 - MS parameters for HCD MS^2, CID MS^2 and CID MS^3 lipid profiling.

Appendix 2: Statistical analysis

Table 12 – Statistical analysis of the lipid class composition in cultures of *P. glacialis* exposed to blue, red and white light.

Lipid class	Comparison	Stad. Dev.	p-value
PC	Red - blue	3.325894	<< 0.05
	Red - white	1.731532	<< 0.05
	Blue - white	1.471675	0.8294251
TG	Red - blue	0.6532735	0.8054816
	Red - white	0.3156732	0.0001744
	Blue - white	0.3625780	0.0000131
MGDG	Red - blue	1.0966014	<< 0.05
	Red - white	0.4173159	<< 0.05
	Blue - white	0.4382712	0.5070972
DG	Red - blue	1.0659052	<< 0.05
	Red - white	0.3535455	<< 0.05
	Blue - white	0.3480071	0.0022962
LPC	Red - blue	0.04633198	<< 0.05
	Red - white	0.03749049	<< 0.05
	Blue - white	0.01570696	<< 0.05
LPE	Red - blue	0.02441215	<< 0.05
	Red - white	0.01706544	<< 0.05
	Blue - white	0.00955444	<< 0.05
PE	Red - blue	0.2970037	0.0140550
	Red - white	0.1989215	0.6425587
	Blue - white	0.1325728	0.0132366
LPG	Red - blue	0.0019423313	0.0004923
	Red - white	0.0008624427	0.0011969
	Blue - white	0.0007774694	0.8342705
MG	Red - blue	0.0038784109	<< 0.05
	Red - white	0.0006854455	<< 0.05
	Blue - white	0.0007019410	0.0095538
PI	Red - blue	0.0004796644	0.0000507
	Red - white	0.0009033753	0.0008536
	Blue - white	0.0017672437	0.1752850
PG	Red - blue	0.2682467	<< 0.05
	Red - white	0.0728611	<< 0.05
	Blue - white	0.1147196	0.1743268

Table 13 – Statistical analysis of EPA content in different lipid classes for cultures of *P. glacialis* exposed to red, blue and white light.

Lipid class	Comparison	Std. Dev.	p-value
PC	Red - blue	3.040999	0.0082548
	Red - white	1.515310	0.0097112
	Blue - white	1.305822	0.9937656
TG	Red - blue	0.11409009	0.0000061
	Red - white	0.08789090	0.9414971
	Blue - white	0.06704568	0.0000001
MGDG	Red - blue	0.3472695	0.0000164
	Red - white	0.1549829	0.0000458
	Blue - white	0.1639988	0.7573378
DG	Red - blue	0.035841219	<< 0.05
	Red - white	0.008437493	<< 0.05
	Blue - white	0.008918811	0.6589282
LPC	Red - blue	0.027906543	<< 0.05
	Red - white	0.023842919	<< 0.05
	Blue - white	0.008886081	<< 0.05
LPE	Red - blue	0.009981663	<< 0.05
	Red - white	0.007550909	<< 0.05
	Blue - white	0.004745355	<< 0.05
PE	Red - blue	0.2591556	0.0522553
	Red - white	0.1850990	0.1829328
	Blue - white	0.1158062	0.6073837
LPG	Red - blue	0.0016388254	0.0265460
	Red - white	0.0007220193	0.0199930
	Blue - white	0.0006574210	0.9798502
PG	Red - blue	0.17808730	0.0005909
	Red - white	0.04684964	0.0032571
	Blue - white	0.08058406	0.5240839
Overall	Red - blue	4.014970	0.0632520
	Red - white	2.030686	0.1218395
	Blue - white	1.756465	0.8743254

Table 14 - Statistical analysis of DHA content in different lipid classes for cultures of *P. glacialis* exposed to red, blue and white light.

Lipid class	Comparison	Std. Dev.	p-value
PC	Red - blue	0.26057528	0.0004549
	Red - white	0.09234562	0.4189206
	Blue - white	0.09469444	0.0003355
TG	Red - blue	0.015912325	0.2148751
	Red - white	0.009442754	0.0823398
	Blue - white	0.007300478	0.7246844
MGDG	Red - blue	0.0012609971	0.2554095
	Red - white	0.0005279360	0.6785792
	Blue - white	0.0004758025	0.5154049
DG	Red - blue	0.010725348	<< 0.05
	Red - white	0.003247338	<< 0.05
	Blue - white	0.003131318	0.0036393
LPC	Red - blue	0.006103901	<< 0.05
	Red - white	0.002874923	<< 0.05
	Blue - white	0.003000209	<< 0.05
LPE	Red - blue	0.013839113	<< 0.05
	Red - white	0.008982504	<< 0.05
	Blue - white	0.004564154	<< 0.05
PE	Red - blue	0.05397374	0.2577080
	Red - white	0.10673535	0.0065064
	Blue - white	0.05397374	0.0391409
PG	Red - blue	0.03896983	0.0000028
	Red - white	0.00742312	0.0000102
	Blue - white	0.01258382	0.6091535
Overall	Red - blue	0.4793376	0.0199132
	Red - white	0.2315795	0.0835623
	Blue - white	0.1797240	0.5793991

Appendix 3: Fragmentation patterns for identification of SQDG

Table 15 - Product ions originating from the sulfoquinovosyl head group, shown with nominal mass.

m/z	Characteristics
81	$[HO_3S]^-$
95	$[CH_3O_3S]^-$
125	$[C_2H_5O_4S]^-$
149	$[C_4H_5O_4S]^-$
153	$[C_4H_9O_4S]^-$
165	$[C_4H_5O_5S]^-$
207	$[C_6H_7O_6S]^-$
225	$[C_6H_9O_7S]^-$
243	$[C_6H_{11}O_8S]^-$
281	$[C_9H_{13}O_8S]^-$
283	$[C_9H_{15}O_8S]^-$
299	$[C_9H_{15}O_9S]^-$

Table 16 – Product ions from fatty acyl chains observed in diatoms. Product ions originating from neutral losses of fatty acids ([M – H-RCOOH]$^-$), neutral losses of aldehyde ([M-H-RCHCO]$^-$) and fatty acids ([RCOOH]$^-$). The m/z values are presented as negatively charged monoisotopic masses calculated by online molecular mass calculators (58). https://www.lfd.uci.edu/~gohlke/molmass/

Fatty acyl chain	m/z [M-H]$^-$	Characteristics
14:0	227.2017	RCOO$^-$
	509.2420	[M-H-RCOOH]$^-$
	527.2526	[M-H-RCHCO]$^-$
16:0	255.2330	RCOO$^-$
	537.2733	[M-H-RCOOH]$^-$
	555.2839	[M-H-RCHCO]$^-$
16:1	253.2173	RCOO$^-$
	535.2577	[M-H-RCOOH]$^-$
	553.2683	[M-H-RCHCO]$^-$
16:2	251.2017	RCOO$^-$
	533.2420	[M-H-RCOOH]$^-$
	551.2526	[M-H-RCHCO]$^-$
16:3	249.1860	RCOO$^-$
	531.2264	[M-H-RCOOH]$^-$
	549.2370	[M-H-RCHCO]$^-$
16:4	247.1698	RCOO$^-$
	529.2107	[M-H-RCOOH]$^-$
	547.2213	[M-H-RCHCO]$^-$
18:0	283.2643	RCOO$^-$
	565.3046	[M-H-RCOOH]$^-$
	583.3152	[M-H-RCHCO]$^-$
18:1	281.2486	RCOO$^-$
	563.2890	[M-H-RCOOH]$^-$
	581.2996	[M-H-RCHCO]$^-$
18:2	279.2330	RCOO$^-$

	561.2733	$[M-H-RCOOH]^-$
	579.2839	$[M-H-RCHCO]^-$
18:3	277.2173	$RCOO^-$
	559.2577	$[M-H-RCOOH]^-$
	577.2683	$[M-H-RCHCO]^-$
18:4	275.2017	$RCOO^-$
	557.2420	$[M-H-RCOOH]^-$
	575.2526	$[M-H-RCHCO]^-$
20:4	303.2330	$RCOO^-$
	585.2733	$[M-H-RCOOH]^-$
	603.2839	$[M-H-RCHCO]^-$
20:5	301.2173	$RCOO^-$
	583.2577	$[M-H-RCOOH]^-$
	601.2683	$[M-H-RCHCO]^-$
22:6	327.2330	$RCOO^-$
	609.2733	$[M-H-RCOOH]^-$
	627.2839	$[M-H-RCHCO]^-$

Appendix 4: Validation of manual identification of SQDG

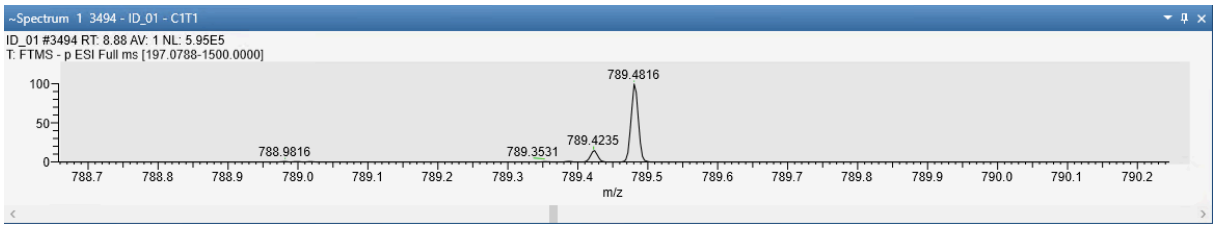

Figure 37 - Isolation window of SQDG 16:2 16:0 from *m/z* 788.7316 to 790.2316, with an interference at *m/z* 789.4235.